# The psychosis risk factor *RBM12* encodes a novel repressor of GPCR/cAMP signal transduction

Received for publication, May 9, 2023, and in revised form, July 20, 2023 Published, Papers in Press, August 4, 2023,
https://doi.org/10.1016/j.jbc.2023.105133

**Khairunnisa M. Semesta**[‡], **Angelica Garces**[‡], **and Nikoleta G. Tsvetanova**[*]
*From the Department of Pharmacology and Cancer Biology, Duke University, Durham, North Carolina, USA*

Reviewed by members of the JBC Editorial Board. Edited by Kirill Martemyanov

***RBM12* is a high-penetrance risk factor for familial schizophrenia and psychosis, yet its precise cellular functions and the pathways to which it belongs are not known. We utilize two complementary models, HEK293 cells and human iPSC-derived neurons, and delineate RBM12 as a novel repressor of the G protein–coupled receptor/cAMP/PKA (GPCR/cAMP/PKA) signaling axis. We establish that loss of RBM12 leads to hyperactive cAMP production and increased PKA activity as well as altered neuronal transcriptional responses to GPCR stimulation. Notably, the cAMP and transcriptional signaling steps are subject to discrete RBM12-dependent regulation. We further demonstrate that the two *RBM12* truncating variants linked to familial psychosis impact this interplay, as the mutants fail to rescue GPCR/cAMP signaling hyperactivity in cells depleted of RBM12. Lastly, we present a mechanism underlying the impaired signaling phenotypes. In agreement with its activity as an RNA-binding protein, loss of RBM12 leads to altered gene expression, including that of multiple effectors of established significance within the receptor pathway. Specifically, the abundance of adenylyl cyclases, phosphodiesterase isoforms, and PKA regulatory and catalytic subunits is impacted by RBM12 depletion. We note that these expression changes are fully consistent with the entire gamut of hyperactive signaling outputs. In summary, the current study identifies a previously unappreciated role for RBM12 in the context of the GPCR–cAMP pathway that could be explored further as a tentative molecular mechanism underlying the functions of this factor in neuronal physiology and pathophysiology.**

G protein–coupled receptors (GPCRs) mediate essential aspects of human physiology and make up the targets of more than a third of all clinically prescribed drugs (1). Because of their vast physiological roles and pharmacological significance, it has been a long-standing goal to identify the factors that regulate GPCR function as these may represent improved targets for therapeutic intervention. Indeed, the main regulatory steps of the cascade are well-characterized. Upon binding to agonist, the receptor stimulates its associated heterotrimeric G protein complex to initiate cell signaling, often via generation of second messengers. Stimulatory receptors, which comprise a large fraction of the GPCR family, couple to Gαs to activate adenylyl cyclases and lead to production of cAMP. The GPCR is then 'shut off' following phosphorylation by G protein-coupled receptor kinases and engagement of arrestins (2). The propagation of the cAMP signal, in turn, is controlled by the interplay between phosphodiesterase (PDE) and effector binding. PKA is one of the main effectors activated by cAMP, and it phosphorylates a myriad of cellular substrates, including the nuclear transcription factor cAMP response-element binding protein (CREB), which stimulates gene transcription (3). Yet, despite these significant advances, much remains to be learned about the mechanisms mediating GPCR function. This has been underscored by the recent discovery that GPCR signaling is compartmentalized through unknown mechanisms (4–7), which has opened new avenues for exploration.

Through a genome-wide CRISPR screen, we identified close to 100 novel regulators of transcriptional signaling downstream of the prototypical Gαs-coupled beta-2-adrenergic receptor (β2-AR) (8). From this screen, RNA-binding motif 12 (RBM12) emerged as one of the most prominent candidate-novel repressor of β2-AR/cAMP signaling. Interestingly, RBM12 has no known ties to GPCR biology. It is annotated as an RNA-binding protein based on co-immunoprecipitation with RNA (9) and based on its amino acid sequence, which is predicted to contain three RNA-recognition motifs (RRMs) (10). In terms of physiology, RBM12 was recently discovered as a high-penetrance risk factor for familial schizophrenia and psychosis in a family-based whole-genome study to identify rare coding sequence variants associated with disease segregation in a pedigree (11). In addition, a different set of mutations in the mouse *RBM12* gene led to neurodevelopmental defects characterized by open mid and forebrain (12). Outside of its functions in the brain, RBM12 was found to be a repressor of fetal hemoglobin expression (9). Therefore, RBM12 is of clear significance for a range of physiologies. Yet, the cellular functions and pathways to which RBM12 belongs are unknown, and therefore it remains unclear how mutations in this gene contribute to disease pathobiology.

In this study, we report a novel mechanism that ties RBM12 to the GPCR/cAMP signaling cascade. In two complementary models, HEK293 cells and human neurons derived from induced pluripotent stem cells (hiPSCs), we demonstrate that loss of RBM12 leads to hyperactive cAMP production,

[‡] These authors contributed equally to this work.
[*] For correspondence: Nikoleta G. Tsvetanova, nikoleta.tsvetanova@duke.edu.

increased PKA activity, and supraphysiological transcriptional signaling in response to β2-AR stimulation. As a result, the compartmentalization of the β2-AR/cAMP signal is compromised. Further, the full repertoire of β2-AR–dependent neuronal transcriptional responses is disrupted by loss of RBM12, leading to overall increase in the extent of gene induction for shared target mRNAs as well as to transcription of distinct targets. We also find that the two *RBM12* truncating mutations linked to familial psychosis are likely loss-of-function, as the mutant proteins fail to rescue GPCR/cAMP signaling hyperactivity in cells depleted of RBM12. Lastly, we present an underlying mechanism for these phenotypes by showing that loss of RBM12 leads to increased expression of multiple adenylyl cyclases and the PKA catalytic subunits and decreased expression of PDE isoforms and a PKA regulatory subunit. In summary, we identify a previously unappreciated role for RBM12 as a repressor of the GPCR/PKA/cAMP signaling axis that is conserved across cell model systems.

## Results

### *RBM12 is a novel repressor of GPCR/cAMP signaling*

In our published genome-wide CRISPR screen, we employed sorting of guide RNA (gRNA)-transduced cells expressing a fluorescent CREB transcriptional reporter following cAMP stimulation through the β2-AR (8). We reanalyzed these data ranking the genes based on "hit strength", defined as the product of the gRNA read count ratio in high versus low fluorescent reporter-expressing sorted fractions and the respective significance *p*-value. With this ranking, RBM12 stood out among the hits, since its depletion gave rise to one of the strongest phenotypes among the candidate novel repressors of the pathway (Fig. 1*A*).

To dissect the functions of RBM12 within the GPCR pathway, we generated clonal KO HEK293 cell lines with CRISPR/Cas9 and two independent gRNAs (Fig. 1*B*). Characterization of the clonal lines showed that they harbored different frameshift mutations resulting in truncated RBM12 protein missing either one (KO 1) or two (KO 2) of its putative RRM domains (Fig. S1, *A* and *B*). β2-AR couples to Gαs to stimulate cAMP production, and therefore we first focused on the effect of RBM12 depletion on cAMP generation. Using a cytosolic luciferase-based biosensor to detect cAMP accumulation in real time in intact cells (13), we found that β2-AR activation led to hyperactive cytosolic cAMP signaling in the two KO lines compared to WT parental cells (Fig. 1*C*). The result was corroborated independently with a high-sensitivity colorimetric immunoassay for cAMP (Fig. S1*C*).

Next, we asked whether the regulatory role of RBM12 is selective for the β2-AR pathway by examining cAMP accumulation downstream of other Gαs-coupled receptors. We observed that stimulation of endogenously expressed adenosine receptors and transfected dopamine 1 receptors led to similarly increased cAMP production in RBM12 KO cells (Figs. 1, *D* and *E* and S1*D*). In contrast, loss of RBM12 did not have a reproducible impact on cAMP inhibition by Gαi-coupled receptors. Specifically, we surveyed the dopamine 2, delta-, and mu-opioid receptors, three prototypical Gαi-coupled GPCRs with important neurobiological functions (14, 15). We found that the inhibitory activity of these receptors did not differ between WT and KO cells (Fig. S1, *F* and *G*). Given that the phenotype was conserved across several Gαs-coupled receptors, we hypothesized that RBM12 may regulate cAMP accumulation also in a GPCR-independent manner. To test this, we activated adenylyl cyclases directly with the drug forskolin, bypassing the receptor activation step, and observed prominent cAMP enhancement in RBM12 KO cells (Fig. 1*F*). Together, these results support RBM12 as a bona fide cAMP signaling repressor and pinpoint a regulatory role at the cAMP accumulation step downstream of GPCR activation.

### *Loss of RBM12 leads to increased PKA activity, supraphysiological transcriptional responses, and impaired compartmentalization of β2-AR signaling*

PKA activation takes place downstream of cAMP production and mediates CREB phosphorylation and CREB-dependent transcriptional signaling. Therefore, to gain a more complete understanding of the functional effects of loss of RBM12 on GPCR/cAMP signaling, we next examined PKA activity and gene expression changes downstream of β2-AR stimulation.

We began by transfecting WT and KO cells with the single-fluorophore excitation PKA biosensor, ExRai-AKAR2. This biosensor undergoes a conformational change upon PKA-dependent phosphorylation leading to increased fluorescence intensity (16). Using microscopy, we detected robust kinase activity in response to isoproterenol across all cell lines. However, RBM12 KOs displayed higher ExRai-AKAR2 activity in comparison to WT ($\Delta F/F_{max}$ = 1.09 ± 0.12 and 0.82 ± 0.06 in the depleted lines versus 0.60 ± 0.07 in the parental line) (Fig. 2*A*). To evaluate the impact on transcriptional signaling, we utilized two complementary assays. First, we quantified accumulation of a fluorescent CREB transcriptional reporter (8) using flow cytometry and found increased β2-AR–dependent reporter accumulation in the KOs (Fig. 2*B*). Next, we used reverse transcription/quantitative PCR (RT-qPCR) analysis of *PCK1* and *FOS* mRNAs, two established endogenous β2-AR transcriptional targets. (17, 18) Similar to the trends observed with the CREB reporter, transcriptional induction of *PCK1* and *FOS* mRNAs was significantly higher in the KOs (Fig. 2, *C* and *D*). Importantly, the results were also reproduced in cells, in which *RBM12* mRNA was depleted acutely by RNAi or CRISPR interference (CRISPRi) (19) (Fig. S2, *A*–*D*). Further, the trends were not selective for the full agonist isoproterenol, as we observed transcriptional hyperactivity after stimulation of KO cells with a panel of endogenous and synthetic partial and full β2-AR agonists (Fig. 2*E*). Based on these data, both receptor-dependent PKA activity and transcriptional signaling are hyperactive in the absence of functional RBM12.

We noted that the extent of β2-AR–dependent transcriptional hyperactivation observed in RBM12 KO cells is striking, especially in the case of *PCK1* mRNA, which we have previously found to be the most robust transcriptional target of the

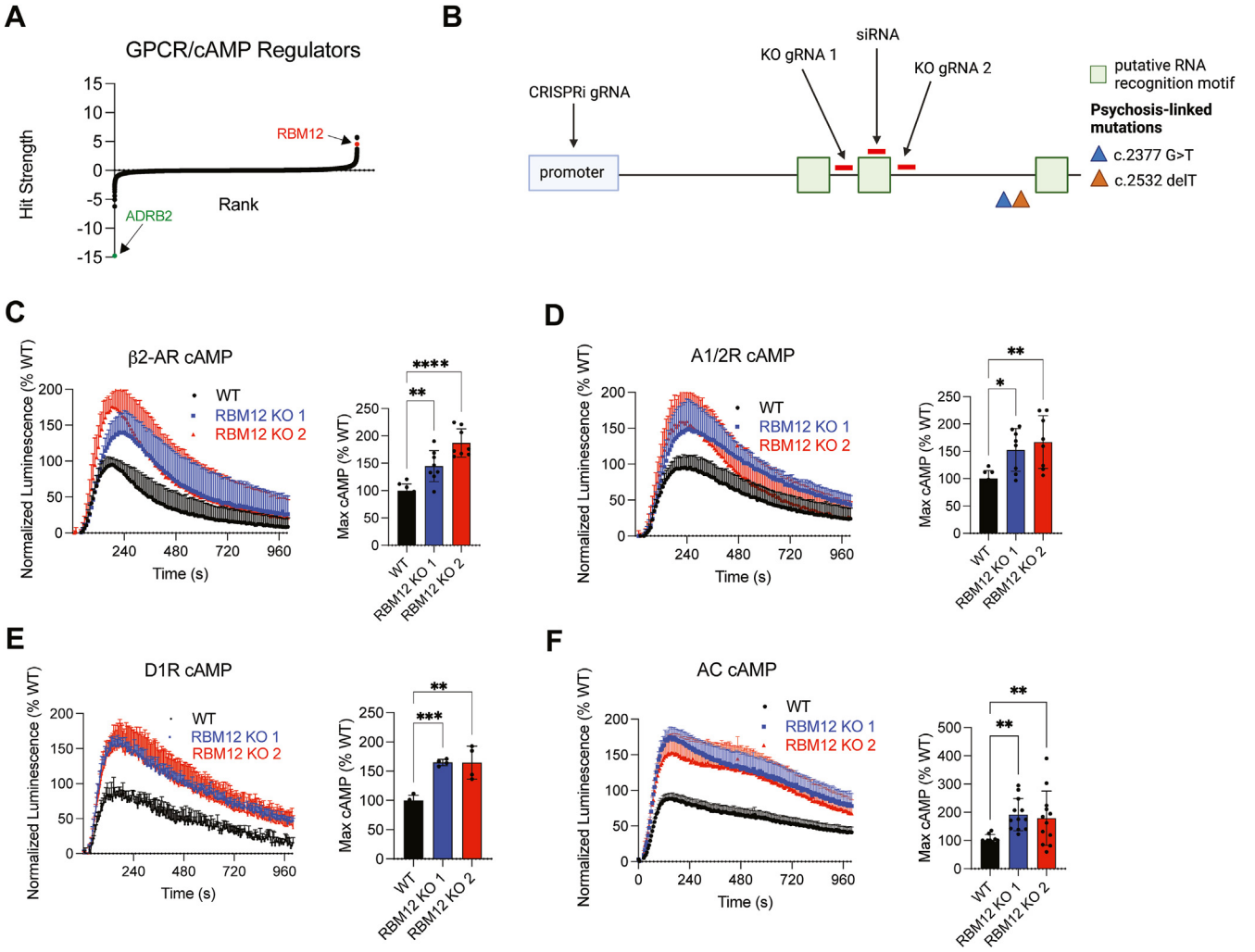


**Figure 1. RBM12 loss leads to hyperactive GPCR/cAMP signaling.** *A*, genes (20,528) ordered by hit strength (product of phenotype score and -$\log_{10}$(*p*-value)). Candidate repressors exhibit hit strength > 0, and candidate activators exhibit hit strength < 0 in a genome-wide CRISPR screen for GPCR/cAMP regulators (8). *B*, schematic of multiple strategies to deplete RBM12 in HEK293 using CRISPRi, RNAi, and CRISPR knockout, depicting positions of guide RNAs, siRNA, and *RBM12* SNPs (c.2377G>T and c.2532delT) implicated in psychosis. *C*, luminescent GloSensor measurement of cAMP accumulation in response to β2-AR agonist isoproterenol (Iso), 100 nM (n = 8). *D*, luminescent GloSensor measurement of cAMP accumulation in response to activation of A1/2R with 10 μM NECA (n = 8). *E*, luminescent GloSensor measurement of cAMP accumulation in response to D1R-selective agonist SKF-81297, 10 nM (n = 4). *F*, luminescent GloSensor measurement of cAMP accumulation in response to direct adenylyl cyclase activation with forskolin, 1 μM (n = 12). All data are mean ± SD. Statistical significance was determined using one-way ANOVA with Dunnett's correction (*C–F*). See also Fig. S1. **** = $p < 0.0001$, *** = $p < 0.001$, ** = $p < 0.01$, * = $p < 0.05$. β2-AR, beta-2-adrenergic receptor; CRISPRi, CRISPR interference; GPCR, G protein–coupled receptor; NECA, 5′-(N-Ethyl Carboxamide) adenosine; RBM, RNA-binding motif.

receptor (∼36–51-fold, Fig. 2*C*) (17). We addressed whether this level of hyperactivation could be recapitulated in WT cells and, if so, under what biological conditions. First, we sought to overexpress the β2-AR reasoning that this would lead to increased cAMP production and transcriptional signaling. We began by expressing the receptor using a weak promoter. Specifically, we amplified a genomic region that included the ∼1 kb sequence upstream of the *ADRB2* ORF, which contains the annotated 5′ UTR and promoter, and the gene coding sequence. We transiently transfected WT cells with the construct and observed that *ADRB2* mRNA levels were notably increased relative to endogenous *ADRB2* in empty vector-transfected cells (∼25-fold increase) (Fig. S2*E*). This resulted in ∼1.3-fold higher isoproterenol-dependent induction of the target mRNA *PCK1*. However, this increased transcriptional response did not match the striking effect seen upon RBM12 depletion (Fig. 2*F*). Next, we expressed the receptor under a CMV promoter leading to dramatically higher *ADRB2* mRNA levels relative to vector-transfected cells (∼1000-fold) (Fig. S2*F*). Under these conditions, β2-AR–dependent *PCK1* mRNA upregulation resembled the levels seen in KO cells (Fig. 2*G*). Based on these results, we hypothesized that loss of RBM12 may mimic a signaling state that can be induced only under supraphysiological activation conditions. To test whether this is indeed the case, we stimulated supraphysiological cAMP in WT cells with the following treatments: (1) saturating isoproterenol in the presence of the PDE4 inhibitor compound rolipram (20) or (2) direct activation of adenylyl cyclase with high doses of forskolin (10 μM). Both activation conditions yielded transcriptional signaling in WT cells that matched the levels observed in the knockouts (Fig. 2, *H* and *I*). Therefore, RBM12 depletion

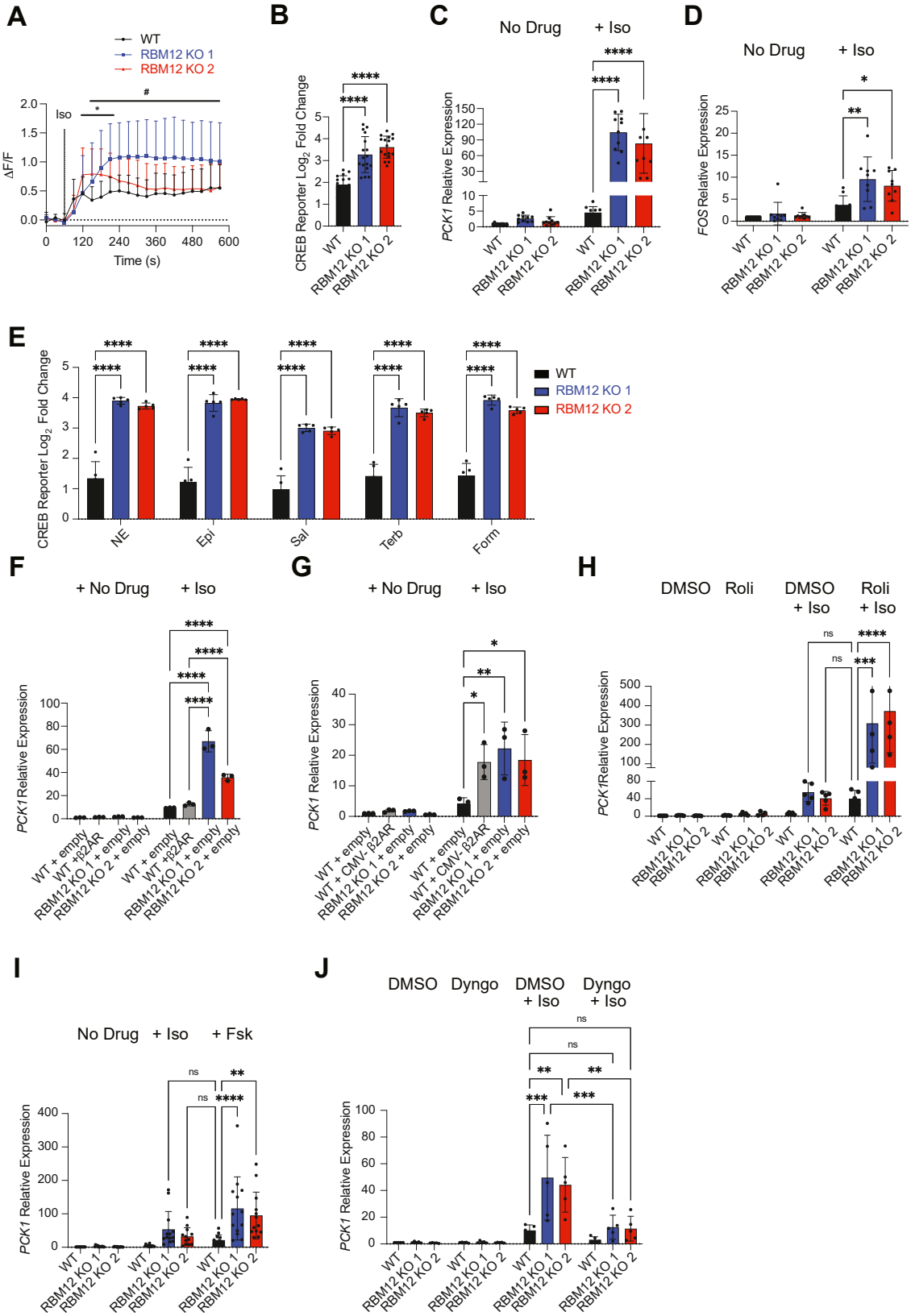


**Figure 2. RBM12 loss leads to increased PKA activity and supraphysiological CREB-dependent transcriptional responses.** *A*, PKA sensor (ExRai-AKAR2) activity in response to 10 nM Iso (n = 24–47 cells from 3-4 independent transfections per cell line). # and * denote statistically significant time points between RBM12 KO1 *versus* WT and KO2 versus WT, respectively. *B*, flow cytometry measurement of fluorescent CREB transcriptional reporter (CRE-DD-zsGreen) in response to 1 μM Iso and 1 μM Shield, 4 h (n = 17). *C*, RT-qPCR analysis of the endogenous β2-AR transcriptional target mRNAs, *PCK1* (n = 10) and (*D*) *FOS* (n = 9) in untreated cells or in cells treated with 1 μM Iso for 1 h. *E*, flow cytometry measurement of the fluorescent CREB transcriptional reporter (CRE-DD-zsGreen) in response to a panel of endogenous (10 μM norepinephrine/NE, 10 μM epinephrine/Epi) or synthetic (10 μM salbutamol/Sal, 10 μM

leads to supraphysiological transcriptional signaling downstream of GPCR activation.

β2-AR signaling was recently found to be compartmentalized, with the β2-AR generating a second wave of signaling from endosomal membranes to selectively induce certain downstream responses. Specifically, the entire repertoire of transcriptional responses was induced by endosomal β2-AR signaling, while plasma membrane receptor activity was effectively uncoupled from this process (17, 21, 22). Given that loss of RBM12 results in higher cAMP and supraphysiological transcriptional responses, we next asked whether the compartmentalization of the GPCR signal may be impaired in the knockouts. To test if plasma membrane–resident β2-ARs may be capable of transducing transcriptional responses upon depletion of RBM12, we acutely blocked receptor internalization into endosomes with the dynamin inhibitor, Dyngo-4a (23). Consistent with previous reports, pretreatment with Dyngo-4a severely abolished *PCK1* mRNA induction by isoproterenol in WT cells (Fig. 2*J*) (17, 21, 22). In marked contrast, β2-ARs confined to the cell surface of RBM12 KO cells stimulated transcriptional responses that were on par with what was observed in WT cells with normal β2-AR trafficking ($\log_2$FC = 3.21 ± 0.32 in vehicle-treated WT cells *versus* $\log_2$FC = 2.94 ± 0.50 and 3.17 ± 0.57 in Dyngo-4a–treated KO cell lines, respectively) (Fig. 2*J*, compare the "WT + Iso/DMSO to "KO + Iso/Dyngo" bars). These responses were further increased in vehicle-treated KO cells stimulated with isoproterenol (Fig. 2*J*). Therefore, while transcriptional responses are orchestrated from endosomal β2-ARs in WT cells, both plasma membrane and endosomal β2-ARs stimulate gene expression when RBM12 is depleted. Importantly, this is not due to differences in receptor trafficking between the cell lines (Fig. S2, *G* and *H*).

### *The cAMP and transcriptional signaling steps are subject to discrete RBM12-dependent regulation*

While we observed that loss of RBM12 impacted the cAMP accumulation and PKA activity steps, it remained to be determined whether hyperactive cAMP production could account for the differences in the downstream responses or whether RBM12 function impacts multiple steps in the pathway.

To address this, we first sought to carefully match isoproterenol activation conditions to yield comparable induced cAMP levels between WT and KO cells and then examined the resulting downstream transcriptional activation. We reasoned that this would allow us to separate the impact of RBM12 depletion on cAMP production from that on downstream transcriptional signaling. Stimulation of knockouts with subsaturating doses of isoproterenol (10 nM) led to cAMP accumulation that was equivalent to that generated by stimulation of the WT with saturating isoproterenol (Fig. S3). Yet, these matched cAMP stimulation conditions still yielded significantly higher transcriptional signaling in RBM12-depleted cells (6.3-9-fold higher *PCK1* mRNA induction compared to WT, $p$-value $< 1.00 \times 10^{-4}$ by one-way ANOVA test) (Fig. 3*A*). To complement these experiments, we next bypassed adenylyl cyclase activation altogether by treating cells with a permeable cAMP analog, 8-CPT-cAMP (24). We observed hyperactive transcriptional signaling in KO cells reflected by increased 8-CPT-cAMP–dependent *PCK1* mRNA induction (Fig. 3*B*). Collectively, these results suggest that cAMP production and transcriptional signaling are independently subject to RBM12 regulation.

### *The neuropsychiatric disease-linked mutations fail to rescue GPCR-dependent hyperactivation in cells depleted of RBM12*

Two truncating variants in the *RBM12* gene (c.2377G>T and c.2532delT) have been implicated as genetic risk factors for familial psychosis (11). However, it is not known how either mutation impacts protein function. We speculated that these mutations may result in nonfunctional RBM12 and therefore impact GPCR/cAMP signaling responses. To test this, we asked whether constructs encoding either WT or variant RBM12 could genetically rescue the hyperactive transcriptional signaling in RBM12-depleted cells. We chose to deplete *RBM12* expression by CRISPRi. Since this approach utilizes a catalytically dead Cas9 fused to a transcriptional repressor to target endogenous promoter regions, it enables rescue with constructs driven by artificial promoters (13). To express RBM12 variants, we cloned lentiviral plasmids encoding N-terminally EGFP-tagged WT, c.2377G>T ('G>T'), or c.2532delT ('delT') RBM12 expressed under the mammalian Ubiquitin C promoter. First, we established that these constructs generated proteins of expected sizes by Western blot. We observed that the two truncating mutations gave rise to smaller protein products. In addition, we noted that the delT variant resulted in reduced protein expression compared to WT and G>T (Fig. 4*A*, compare lanes 1 and 2 to lane 3). We did not observe downregulation in delT mRNA levels (Fig. S4*A*), suggesting that the mutation impacts a posttranscriptional step, either protein translation or stability. Next, we tested whether the mutant proteins displayed altered subcellular localization. Studies done in primary human erythroblasts, A-431, and U-2OS cells found that RBM12 displayed nuclear localization (9, 25). In agreement with these reports, we observed nuclear localization for native RBM12 under both basal and isoproterenol-induced conditions in

terbutaline/Terb, 50 nM formoterol/Form) β2-AR agonists and 1 μM Shield for 4 h (n = 5). *F* and *G*, *PCK1* mRNA expression in untreated or 1 μM Iso-treated cells transfected with empty plasmid (n = 3), (*F*) plasmid construct expressing lower levels of β2AR (n = 3), or (*G*) plasmid expressing β2AR from a CMV promoter (n = 3). *H*, *PCK1* mRNA expression in untreated or 1 μM Iso-treated cells for 1 h in the presence of either vehicle (DMSO) or 10 μM of the PDE4 inhibitor Rolipram (n = 4–5). *I*, RT-qPCR of *PCK1* mRNA in untreated cells or cells treated with 1 μM Iso-treated cells or 10 μM forskolin for 1 h (n = 12–13). *J*, *PCK1* mRNA expression in cells pretreated with either vehicle (DMSO) or 30 μM Dyngo-4A for 20 min, then treated with 1 μM Iso for 1 h (n = 5). All data are mean ± SD. Statistical significance was determined using multiple unpaired *t*-tests with Benjamini, Krieger and Yekutieli false discovery rate correction (*A*), one-way ANOVA with Dunnett's correction (*B*), or two-way ANOVA with Tukey's correction (*C–J*). See also Fig. S2. **** = $p < 0.0001$, *** = $p < 0.001$, ** = $p < 0.01$, * = $p < 0.05$. β2-AR, beta-2-adrenergic receptor; PDE, phosphodiesterase; RBM, RNA-binding motif.

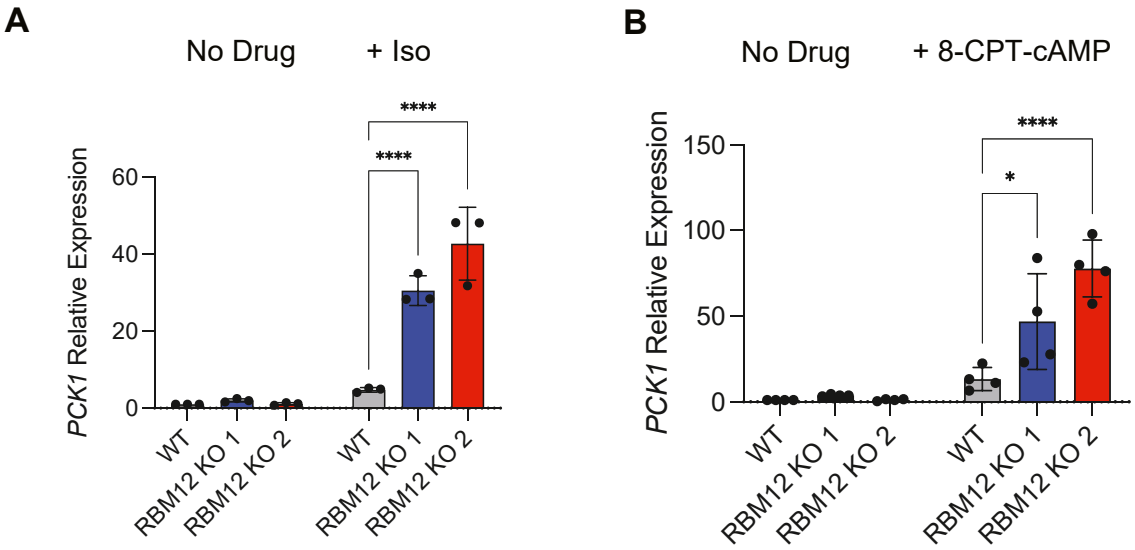


**Figure 3. RBM12 impacts the cAMP and transcriptional signaling steps independently.** *A*, *PCK1* mRNA expression in untreated cells or in cells treated with either 1 μM isoproterenol (WT cells) or 10 nM isoproterenol (RBM12 KO cells) for 1 h (n = 3). *B*, *PCK1* mRNA expression in untreated cells or in cells treated with 150 μM 8-CPT-cAMP for 1 h (n = 4). All data are mean ± SD. Statistical significance was determined using two-way ANOVA with Tukey's correction (*A* and *B*). See also Fig. S3. **** = $p < 0.0001$, * = $p < 0.05$. RBM, RNA-binding motif.

HEK293 cells (Fig. 4*B*). Similarly, WT EGFP-RBM12 localized to the nucleus (Fig. 4*C*, top panel). The truncating mutations did not perturb protein localization as both the G>T and delT variants also concentrated in the nucleus (Fig. 4*C*, middle and bottom panels).

We proceeded to evaluate whether the mutants could rescue the hyperactive GPCR/cAMP signaling phenotype seen in RBM12-depleted cells. We simultaneously transduced HEK293 cells stably expressing dCas9-KRAB with (1) either a nontargeting control (NTC) gRNA or a gRNA against *RBM12* and (2) an empty EGFP backbone, WT, G>T, or delT *RBM12* constructs. To monitor CREB-dependent transcription, we generated a new version of the CREB transcriptional reporter, in which cAMP responsive elements drive the production of a red fluorescent protein in response to cAMP accumulation. This allowed us to selectively examine reporter levels in cells that express the CRISPRi gRNA (tagged with BFP) and the RBM12 constructs (tagged with EGFP) by flow cytometry (Figs. 4*D* and S4, *B* and *C*). As expected, we observed increased reporter accumulation upon isoproterenol stimulation in *RBM12* gRNA-transduced compared to NTC-transduced cells (Fig. 4*E*, leftmost black vs red bars). Notably, we found that normal signaling downstream of β2-AR activation was restored only in cells expressing WT, but not the G>T or delT mutant (Fig. 4*E*). Therefore, neither of the two disease-linked RBM12 variants could rescue impaired GPCR-dependent signaling.

### *RBM12 is a repressor of GPCR/cAMP signaling in hiPSC-derived neurons*

RBM12 is expressed ubiquitously across different tissues (26). However, it likely has important functions in the brain based on its ties to neuropsychiatric disorders (11) and neurodevelopment (12). Therefore, to examine the role of RBM12 in GPCR/cAMP signaling in a physiologically relevant model, we chose hiPSC-derived neurons (iNeurons). iNeurons offer a unique setting to investigate receptor activity in live human neurons and a suitable genetic context to study the functional effects of disease-relevant gene mutations. Since glutamatergic signaling is of key significance in the pathobiology of neuropsychiatric diseases, including schizophrenia (27–31), we selected a previously published clonal hiPSC line harboring an inducible Neurogenin 2 (*NGN2*) driven by a doxycycline-inducible promoter for glutamatergic differentiation (32). In addition, this line expresses dCas9-KRAB-BFP and is therefore compatible with CRISPRi-based gene silencing (Fig. 5*A*). The hiPSC-derived neuronal line expresses low levels of endogenous β2-ARs, leading to very modest induction of cAMP and transcriptional signaling. In order to achieve responses that are robust enough to be accurately captured by the cAMP sensor and gene expression assays, we chose to overexpress the receptor in the hiPSC line and sorted cells with moderate β2-AR levels (~20-fold increase relative to native mRNA levels, Fig. S5*A*). We noted that, when overexpressed to similar extent in HEK293 cells, β2-AR does not lead to supraphysiological pathway activation upon stimulation with agonist (Fig. S2, *I* and *J*). In this hiPSC line, we observed nuclear staining of native RBM12 under both basal and isoproterenol-induced conditions in neurons, consistent with its localization in HEK293 cells (Fig. 5*B*). To deplete *RBM12*, we utilized either NTC or *RBM12*-targeting gRNAs, sorted the gRNA-transduced cells, and confirmed *RBM12* mRNA depletion by qPCR and protein expression by Western blotting (Fig. S5*B*). Importantly, we verified that these cells expressed comparable levels of FLAG-β2-AR upon differentiation into iNeurons (Fig. S5*C*).

We began by differentiating hiPSCs with doxycycline for 2 weeks and examining the impact of *RBM12* depletion on cAMP accumulation. We used an established fluorescent

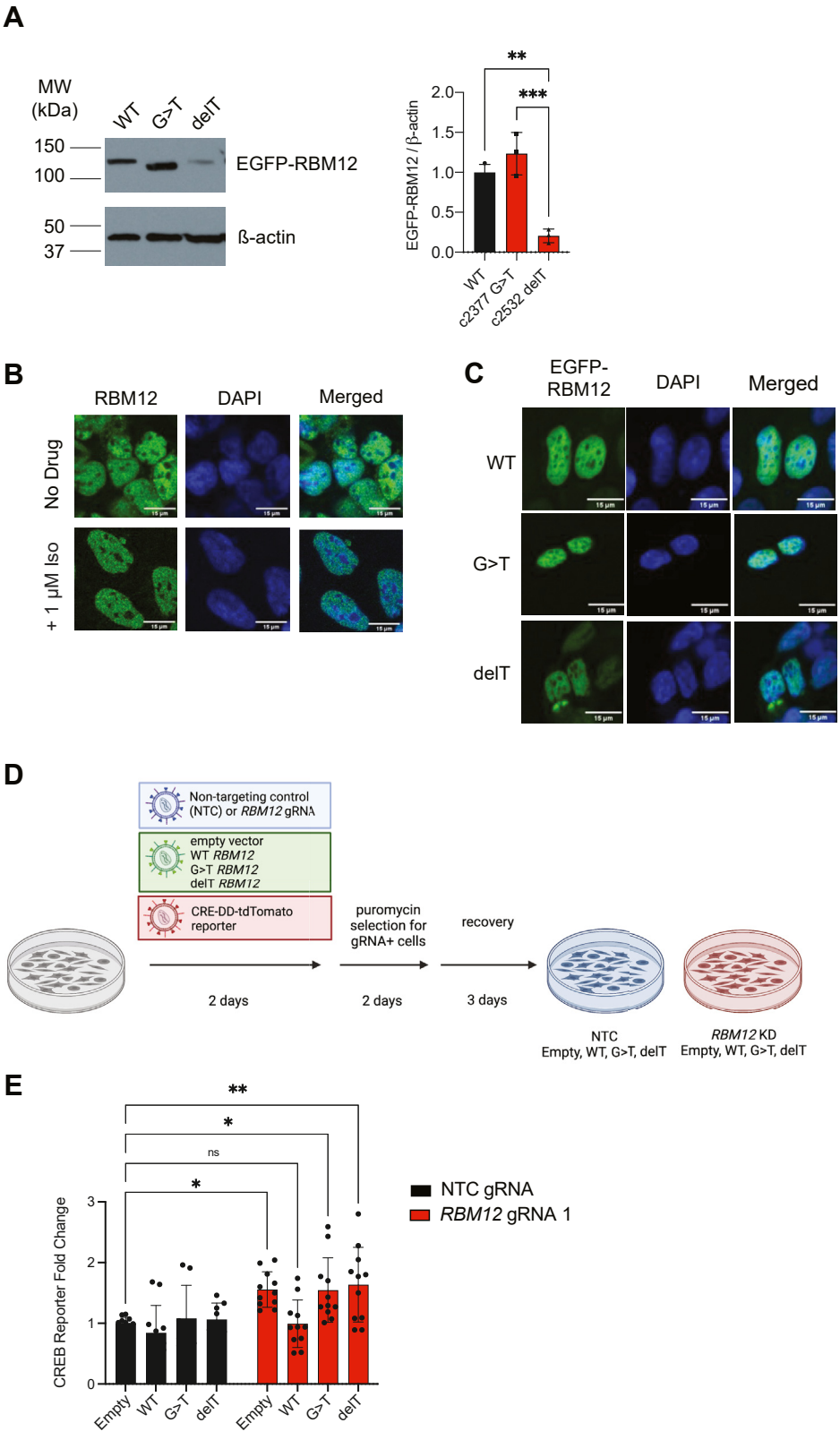


**Figure 4. Expression of disease-associated variants in RBM12 knockdown cells does not rescue the hyperactive GPCR-dependent transcriptional signaling.** *A*, Western blot analysis of EGFP-tagged WT, c.2377G>T and c.2532delT RBM12 (n = 3) probed with antibody recognizing EGFP. All data are normalized relative to WT. See also Fig. S7. *B*, fixed cell fluorescence microscopy analysis of endogenous RBM12 in untreated and stimulated (1 µM Iso for 20 min) HEK293 cells. *C*, localization of EGFP-tagged WT, c.2377G>T or c.2532delT RBM12 by fluorescence microscopy. *D*, schematic of the flow cytometry–based rescue experiment. *E*, flow cytometry measurement of the fluorescent CREB transcriptional reporter (CRE-DD-tdTomato) in response to 1 µM Iso and 1 µM Shield for 6 h (n = 8–11). Data are normalized relative to the "NTC + empty vector" sample values. All data are mean ± SD. Statistical significance was determined using one-way ANOVA (A) or two-way ANOVA with Dunnett's correction (*E*). See also Fig. S4. *** = $p < 0.001$, ** = $p < 0.01$, * = $p < 0.05$. GPCR, G protein–coupled receptor; NTC, nontargeting control; RBM, RNA-binding motif.

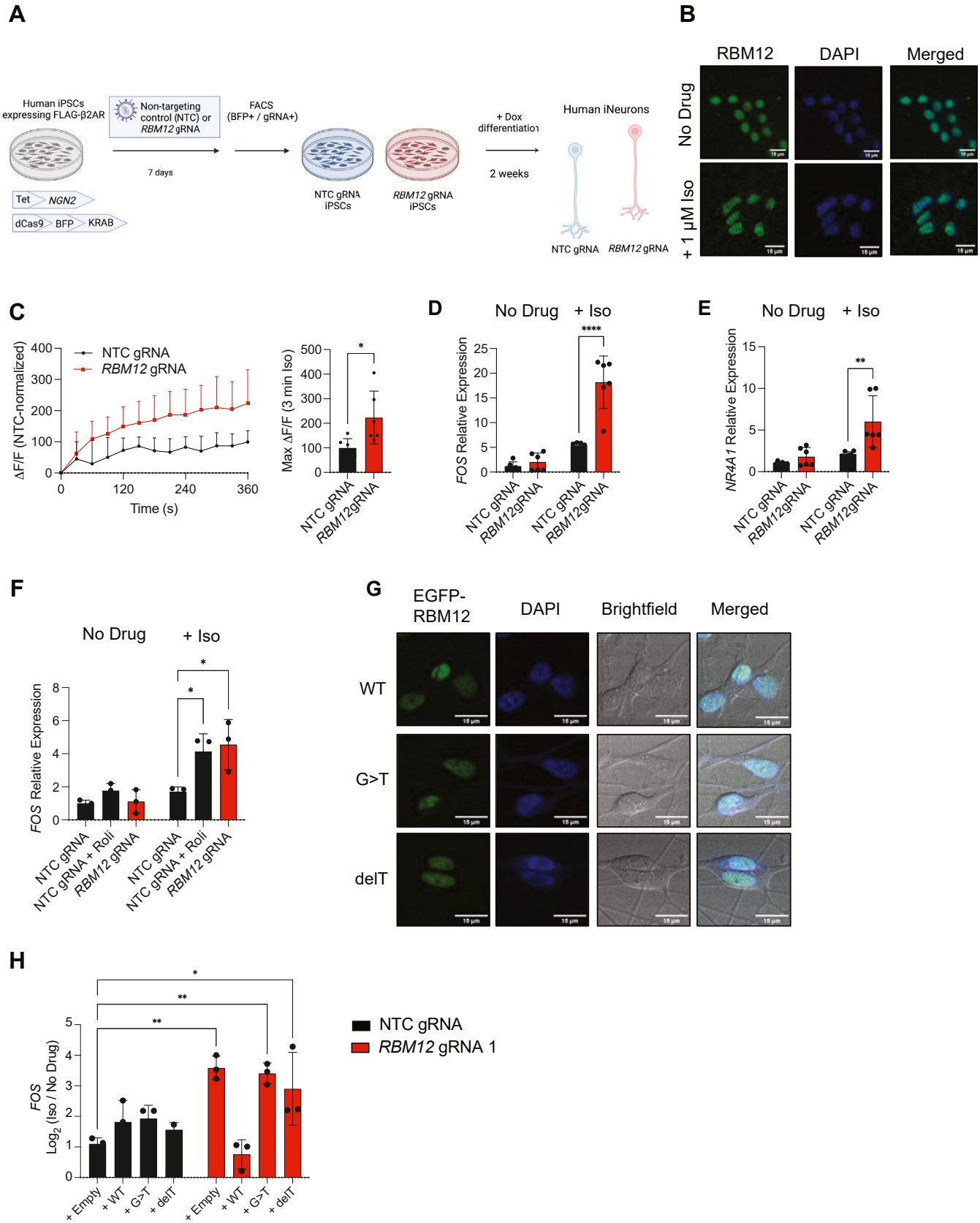


**Figure 5. Signaling hyperactivity upon loss of RBM12 in human iPSC-derived neurons.** *A*, schematic of the CRISPRi-mediated RBM12 depletion in human iPSC-derived neurons. *B*, fixed cell fluorescence microscopy imaging of native RBM12 in untreated and stimulated (1 µM Iso for 30 min) iNeurons. *C*, accumulation of the fluorescent cADDis sensor in NTC- and *RBM12* gRNA-expressing neurons in response to 1 nM Iso (n = 6). *D*, expression of *FOS* and (*E*) *NR4A1* mRNAs in response to treatment with 1 µM Iso for 1 h by RT-qPCR (n = 6). *F*, expression of *FOS* mRNA in response to 1 µM Iso in the presence of either vehicle (DMSO) or 10 µM Rolipram in neurons treated for 1 h (n = 3). *G*, expression of EGFP-tagged WT, c.2377G>T or c.2532delT RBM12 by

cytosolic cAMP biosensor, cADDis (33). We found that iNeurons transduced with *RBM12* gRNA exhibited hyperactive cAMP signaling upon β2-AR activation relative to NTC-harboring iNeurons (Fig. 5*C*). To examine transcriptional responses, we utilized RT-qPCR analysis of *NR4A1* and *FOS* mRNAs, two known CREB-dependent immediate early genes induced by neuronal activity (34–37). We saw that *RBM12* knockdown yielded hyperactive upregulation of both mRNAs (Fig. 5, *D* and *E*). Notably, the extent of transcriptional hyperactivity seen in the knockdown could be recapitulated in NTC-harboring cells under supraphysiological cAMP activation with isoproterenol and rolipram (Fig. 5*F*). Lastly, we assessed whether the two RBM12 mutants could rescue the impaired signaling phenotype. WT, G>T, and delT RBM12 transduced into iNeurons localized to the nucleus (Fig. 5*G*). In agreement with the expression trends seen in HEK293, we observed reduced delT mutant protein but not mRNA expression compared to WT or G>T RBM12 (Fig. S5, *D* and *E*). RBM12-dependent hyperactive transcriptional signaling was abolished upon expression of WT RBM12, but not G>T or delT, as evaluated by RT-qPCR analysis of *FOS* mRNA (Fig. 5*H*). Thus, depletion of *RBM12* in human neurons recapitulates the gamut of signaling phenotypes seen in HEK293. Collectively, these results support conserved RBM12-dependent regulation of the GPCR/cAMP pathway across cell types, including in a physiologically relevant system.

### *β2-AR activation in RBM12-depleted cells leads to modified neuronal transcriptional responses*

To capture the cellular functions impacted by *RBM12* depletion, we carried out genome-wide transcriptomic analysis of untreated and isoproterenol-activated NTC- and *RBM12* gRNA-expressing iNeurons. We began by defining a set of all possible β2-AR–dependent transcriptional targets across the two neuronal lines. For this analysis, we independently identified target sets in NTC-transduced ("wild-type") and *RBM12* knockdown neurons by differential expression analysis between each respective basal and isoproterenol conditions. We obtained a total of 669 unique β2-AR–dependent transcriptional targets across the two cell lines (Fig. 6*A* and Table S1). We observed a statistically significant enrichment of known endogenous β2-AR transcriptional targets (17) ($p < 1.0 \times 10^{-41}$ by Fisher's exact test) and CREB targets (38) ($p < 1.0 \times 10^{-26}$ by Fisher's exact test) in this dataset. To elucidate specific β2-AR–dependent neuronal processes, we performed gene ontology (GO) term analysis of the targets (39). We identified a breadth of regulated processes including metabolic processes, cell differentiation, response to hormone/stimulus, regulation of gene expression, learning and memory, and neuronal differentiation (FDR $p_{adj} < 5.0 \times 10^{-2}$ by Fisher's exact test) (Fig. 6*B*). Importantly, at least 110 genes associated with neuronal activity, memory, cognition, as well as synaptic transmission and synapse formation were represented among the β2-AR–dependent targets (37). These included brain-derived neurotrophic factor (*BDNF*) and transcription factor–coding genes (*e.g.*, *NR4A1, FOS, FOSB, EGR1, JUN*), consistent with the reported critical roles of the β2-AR–cAMP pathway in neurobiology (Table S1) (40).

Under basal conditions, we did not observe any notable trends toward RBM12-dependent increase in the expression of the targets (Fig. S6*A*). However, under isoproterenol stimulation, we found significant transcriptional hyperactivation across all target genes in the *RBM12* knockdown ($p < 2.2 \times 10^{-16}$ by Wilcoxon signed rank test). We also found that the expression changes for these transcriptional targets are strongly correlated between neurons expressing moderate β2-AR levels and the isogenic parental neurons expressing native β2-ARs (Pearson coefficient = 0.64, $p < 1.0 \times 10^{-4}$, Fig. S6*B*), demonstrating that these indeed represent bona fide targets. To gain deeper insight into these differences, we next asked how many of the targets are selectively induced in response to β2-AR stimulation in each cell line. In principle, genes may be upregulated in either WT or *RBM12* knockdown, representing qualitatively distinct targets. On the other hand, targets may be changing in both WT and *RBM12*-depleted neurons but to different extent (quantitatively distinct targets). To identify qualitatively unique targets for each cell line within the set of 669 genes, we applied a cut-off of gene $\log_2$-fold change $\geqq 0$ with isoproterenol in one neuronal line but not the other. This analysis yielded 21 WT- and 115 *RBM12* knockdown-specific target genes (Table S1). Interestingly, genes with known functions in synapses, memory, and cognition were represented in both exclusive lists. Factors involved in synaptic plasticity such as *JUN, ARC* (encoding the activity-regulated cytoskeleton-associated protein), *BDNF*, and *NRXN3* (encoding the cell adhesion molecule neurexin-3-alpha) were induced only in *RBM12* knockdown neurons. While the remaining 533 genes were induced in both cell lines, there was a significant trend toward RBM12-dependent hyperactivation ($p < 2.2 \times 10^{-16}$ by Wilcoxon signed rank test). These results indicate that the neuronal β2-AR–dependent transcriptome is disrupted by *RBM12* depletion, resulting in both quantitatively and qualitatively distinct responses.

### *RBM12 impacts GPCR/cAMP signaling through regulation of adenylyl cyclase and PKA expression*

RBM12 is localized in the nucleus (Fig. 4*B*) and was recently shown to have RNA-binding activity (4). Yet, loss of RBM12 impacts multiple signaling steps, including cAMP production which takes place in the cytosol. Thus, we speculated that the observed regulation may take place through other factor(s) that in turn are dependent on RBM12 for proper expression or function. To begin to dissect the mechanisms governing the RBM12-dependent regulation of GPCR signaling, we

fluorescence microscopy. *H*, expression of *FOS* mRNA in response to stimulation with 1 μM Iso for 1 h in neurons transduced with empty plasmid or plasmid encoding WT, G>T, or delT EGFP-RBM12 (n = 2–3). All data are mean ± SD. Statistical significance was determined using unpaired two-sided Student *t* test (C) or two-way ANOVA with Tukey's correction (*D–F*, and *H*). See also Fig. S5. **** = $p < 0.0001$, ** = $p < 0.01$, * = $p < 0.05$. CRISPRi, CRISPR interference; NTC, nontargeting control; RBM, RNA-binding motif.

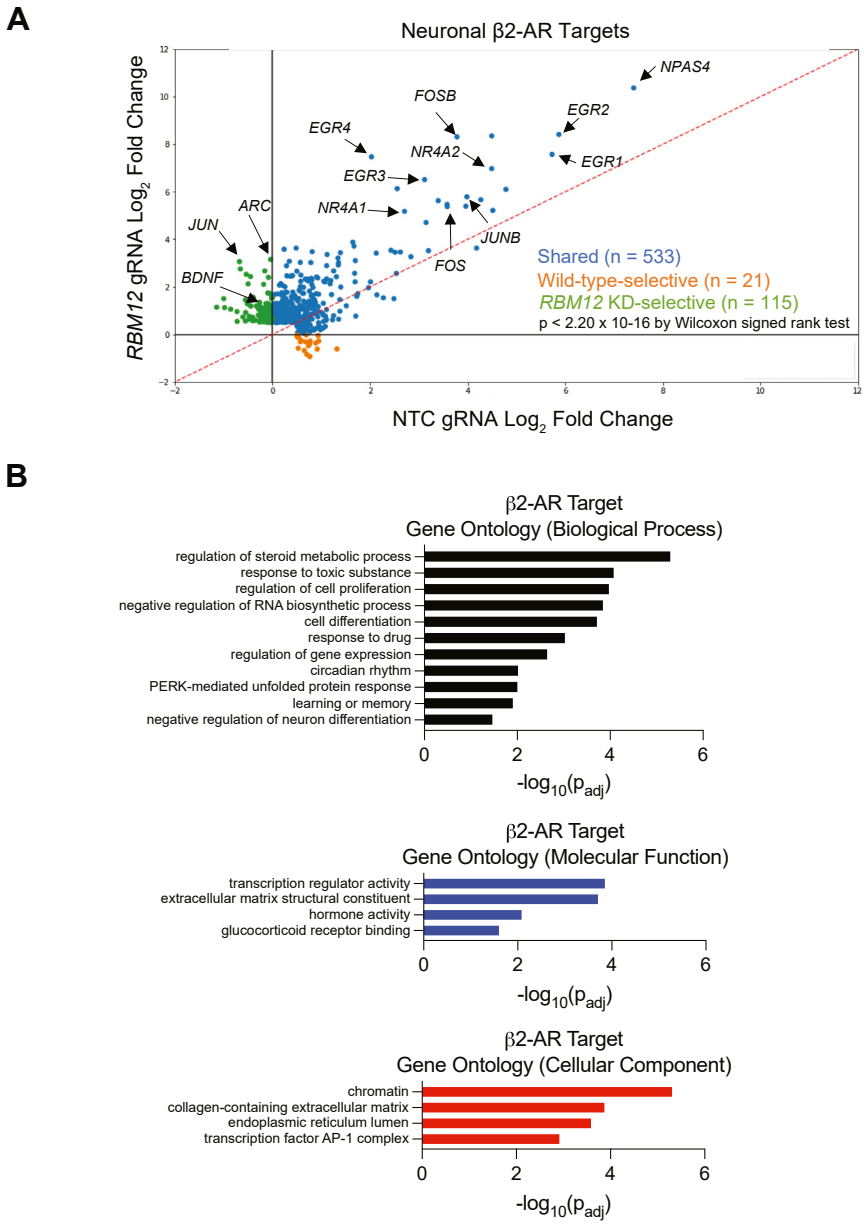


**Figure 6. RBM12 loss impacts the β2-AR neuronal transcriptional responses**. *A*, scatter plot showing gene fold induction ($log_2$ Iso/no drug) of neuronal β2-AR targets (n = 669) identified by RNA-seq analysis (n = 3 per cell line per drug condition). *Blue* dots represent genes that were induced by a 1-h treatment with 1 μM Iso in both WT (NTC gRNA) and *RBM12* KD (*RBM12* gRNA) neurons. *Orange* dots represent genes that were induced only in WT and unchanged or downregulated in *RBM12* KD neurons. *Green* dots represent genes that were induced only in *RBM12* KD neurons and unchanged or downregulated in WT. Indicated by *arrows* are a subset of genes with established roles in neuronal activity. The underlying information is summarized in Table S1. *B*, gene ontology categories enriched among the neuronal β2-AR targets from (*A*). Statistical significance was determined using Wilcoxon signed rank test (*A*) and Fisher's exact test (*B*). See also Fig. S6. β2-AR, beta-2-adrenergic receptor; NTC, nontargeting control; RBM, RNA-binding motif.

performed differential expression analysis between untreated WT and untreated *RBM12*-depleted neurons. We identified 2645 differentially expressed genes (Table S2). GO analysis identified processes related to nervous system development and function as well as "GPCR signaling pathway" and "adenylyl cyclase–modulating signaling pathway" (Fig. 7*A* and Table S2). We were particularly intrigued by the latter GO term categories, as they could provide insights into the identity of the proximal regulator(s) of our pathway. We found altered expression of several effectors with known roles in the GPCR/cAMP cascade, including adenylyl cyclases, PDEs, and PKA isoforms (Table S2). We sought to further narrow down the factors by identifying effectors that display consistent RBM12-dependent abundance changes in both iNeurons and HEK293 cells. For that, we carried out transcriptomic analysis of the HEK293 KO and parental lines and compared the list of differentially expressed genes between model systems to find shared cAMP pathway effectors. For genes expressed in both models, we required that (1) factor abundance changes trended in agreement in the neuron and HEK293 experiments and (2) these changes were statistically significant ($p_{adj} < 5.0 \times 10^{-2}$ by Wald test) in at least two out of the three depleted cell line

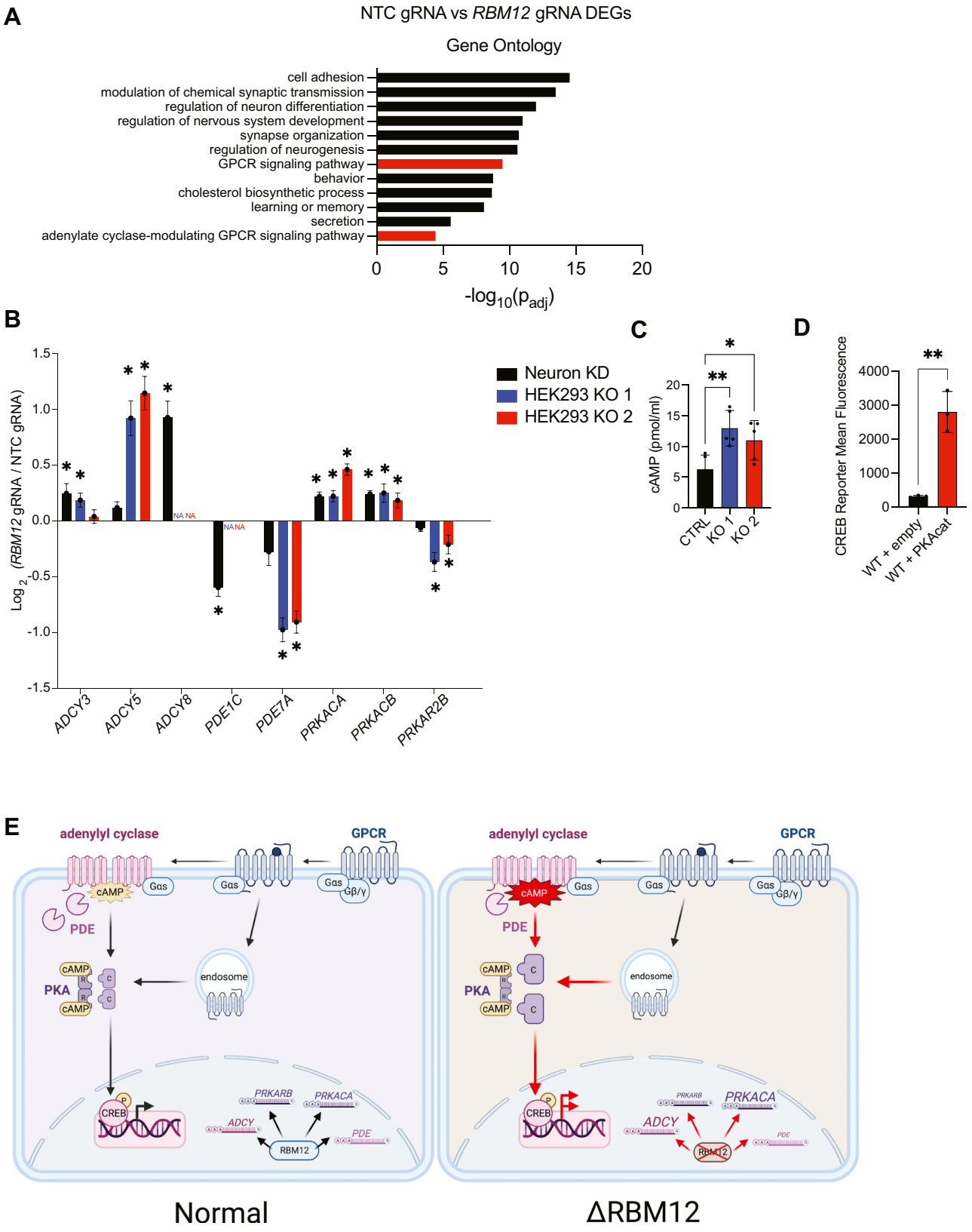


**Figure 7. RBM12 regulates the expression of multiple GPCR/cAMP effectors.** *A*, gene ontology analysis of differentially expressed genes between WT and *RBM12* KD neurons (n = 2645 genes). *B*, graph summarizing abundance changes ($log_2$ fold change RBM12 gRNA/NTC gRNA) of known GPCR/cAMP regulators in WT and *RBM12* KD neurons (n = 3 per cell line) and HEK293 (n = 7 in WT cells and n = 3 per KO cell line). Asterisks denote statistical significance ($p_{adj} < 5.0 \times 10^{-2}$ by Wald test). "NA" denotes genes not expressed in HEK293. *C*, basal cAMP levels in WT and HEK293 RBM12 KOs measured using ELISA assay (n = 5). All values are normalized relative to WT. *D*, flow cytometry measurement of the fluorescent CREB transcriptional reporter (CRE-DD-zsGreen) in WT cells expressing either empty plasmid or plasmid encoding PKAcat following stimulation with 1 μM Iso and 1 μM Shield for 4 h (n = 3). *E*, model of RBM12-dependent regulation of the GPCR/cAMP signaling pathway. All data are mean ± SD. Statistical significance was determined using Fisher's exact test

models. As a result, we found that two adenylyl cyclase isoforms (*ADCY3* and *ADCY5*) were consistently upregulated, while *PDE7A* was downregulated (Fig. 7*B*). In addition, the abundance of the neuron-specific *ADCY8* and *PDE1C* was aberrant: *ADCY8* levels were increased, while *PDE1C* levels were decreased upon *RBM12* depletion in neurons (Fig. 7*B*). The fact that *ADCY* abundance was higher in *RBM12*-depleted cells suggests that, in addition to stimulated cAMP, basal cAMP levels may also be increased. Indeed, we found that cAMP concentrations were significantly elevated in untreated RBM12 KO relative to WT HEK293 cells (Fig. 7*C*). In contrast, loss of RBM12 did not consistently impact the basal levels of another second messenger, cGMP (Fig. S6*C*), or the expression of soluble guanylyl cyclases across our cell models (Fig. S6*D*).

We also found that the expression of *PRKACA* and *PRKACB*, which encode the PKA catalytic (PKAcat) subunits Cα and Cβ, was upregulated in RBM12-depleted cells (Fig. 7*B*). On the other hand, the expression of *PRKAR2B*, which encodes the PKA type II-beta regulatory subunit (RIIβ), was downregulated in RBM12-depleted cells (Fig. 7*B*). Mirroring the trends in mRNA, the protein levels of the PKAcat isoform predominantly expressed in most tissues (41, 42), Cα, were also higher in both RBM12 KO HEK293 cells and in neurons acutely depleted of *RBM12* by CRISPRi (Fig. S6, *E* and *F*). To test whether PKA overexpression alone is sufficient to induce hyperactive downstream transcription, we transiently expressed PKAcat in WT HEK293 cells and measured fluorescent CREB reporter levels. We found that β2-AR–dependent accumulation of the reporter was indeed higher in cells transfected with PKAcat (Fig. 7*D*). Therefore, the RBM12-dependent transcriptional hyperactivity, including following cascade stimulation with a cAMP analog (Fig. 3*B*), could be driven at least in part by increased expression of PKAcat. Collectively, the transcriptomic changes induced by loss of RBM12 are consistent with the hyperactive GPCR/cAMP/PKA signaling phenotypes and support impaired *ADCY*, *PDE*, and *PRKACA* abundance as an underlying molecular mechanism.

## Discussion

In this study, we identify and characterize RBM12 as a novel repressor of GPCR/cAMP signaling. Although mutations in *RBM12* have been linked to heritable psychosis and neurodevelopmental defects (11, 12), its precise cellular functions are not well-understood. We discover that RBM12 independently impacts multiple steps within the GPCR–cAMP pathway. Loss of RBM12 leads to hyperactive basal and stimulated cAMP (Figs. 7*C* and 1*C*) as well as increased PKA activity and transcriptional signaling upon activation of the β2-AR and direct activation of adenylyl cyclases with forskolin (Figs. 1 and 2).

RBM12 is predominantly localized to the nucleus (25) and has been shown to bind RNA and to tentatively impact transcript splicing (9). Based on the present work, we cannot rule out that the cytosolic fraction of RBM12 plays a direct regulatory role in GPCR signaling. Studies aimed at defining the RBM12 interactome could resolve this possibility. However, we favor a more parsimonious model, according to which nuclear RBM12 controls the transcriptional or post-transcriptional fate of cytosolic factors that in turn directly impact the GPCR pathway (Fig. 7*E*). In support of this, we demonstrate that loss of RBM12 leads to impaired expression of multiple factors of established significance within the GPCR/cAMP cascade, including adenylyl cyclases, PDEs, and PKA regulatory and catalytic subunits (Fig. 7*B*). Upon RBM12 depletion, PKA RIIβ levels are decreased, while Cα and Cβ levels are increased. These results are intriguing in the context of our current understanding of how PKAcat diffusion may be limited in cells. The PKA regulatory subunits are in large molar excess of the catalytic subunits in a wide range of tissues, including in the brain, facilitating efficient 'recapture' of liberated catalytic subunits (43). Based on this, we speculate that depletion of RBM12 likely leads to reduced anchoring of PKAcat and therefore to loss of compartmentalized PKA activity. Impaired compartmentalization of GPCR and cAMP signaling would be expected to arise also from the altered adenylyl cyclase and PDE abundance in *RBM12*-depleted cells. Several *ADCY* genes are upregulated, while *PDE* isoforms are downregulated in *RBM12* knockdowns (Fig. 7*B*). Indeed, we report that transcriptional signaling, a cellular response downstream of the β2-AR that is known to be spatially encoded (17, 21, 22), is compromised in the knockout (Fig. 2*J*). Moreover, the hyperactive transcriptional response seen in the mutant can be recapitulated only under supraphysiological activation conditions, including PDE inhibition and receptor overexpression (Fig. 2, *G* and *H*), which are expected to abolish compartmentalized signaling (17, 44, 45). Future studies that apply cAMP and PKA biosensors targeted to distinct subcellular organelles would be invaluable in further defining local signaling in RBM12 knockouts. It is also important to note that our experiments do not directly address or establish whether the RBM12-dependent regulation of cAMP arises downstream of transmembrane adenylyl cyclases, the soluble adenylyl cyclase, or both. Since we detect significantly impacted expression of transmembrane adenylyl cyclase in the KO lines, we hypothesize that these isoforms likely play primary roles in the context of the regulation. However, these pathways are intricately interconnected and therefore a rigorous dissection of the contributions of each cyclase constitutes another important avenue for future investigation that will shed light onto the regulatory interplay between RBM12 and GPCR/cAMP signaling.

Two mutations in the *RBM12* gene (c.2377G>T and c.2532delT), each resulting in the truncation of the terminal RRM domain, were recently associated with familial psychosis (11). Here, we observe that the delT protein is expressed at

(*A*), adjusted *p*-value corrected for multiple testing by Wald test (*B*), one-way ANOVA with Dunnett's correction (*C*), or unpaired two-sided Student *t* test (*D*). ** = $p < 0.01$, * = $p < 0.05$. GPCR, G protein–coupled receptor; RBM, RNA-binding motif; NTC, nontargeting control; PKAcat, PKA catalytic.

decreased levels compared to WT or G>T RBM12 (Figs. 4*A*, S4*B*, and S5*D*). We further find that neither variant can rescue aberrant GPCR/cAMP signaling when expressed in HEK293 cells and neurons depleted of RBM12 (Figs. 4*E* and 5*H*). Accordingly, the two mutations lead to loss-of-function protein likely through distinct mechanisms. While the delT-related phenotypes may stem at least in part from diminished protein expression, the G>T mutation may interfere with RBM12 function by abolishing interactor binding. Interestingly, the last RRM domain does not appear to be required for all processes regulated by RBM12. A recent study found a novel role of RBM12 as a repressor of fetal hemoglobin expression (9). Notably, the authors reported a requirement only for the N-terminal portion of the protein in that process, whereas deletion of the C-terminal RRM domain, which is truncated in the psychosis cohorts, was dispensable from that regulation. Therefore, the C-terminal RRM domain and its interactome must be of particular significance in the context of RBM12 and its role in GPCR/cAMP signaling. We note that our study is limited by the overexpression of RBM12 variants in a genetically depleted background and thus may not fully recapitulate the consequences of the disease-relevant mutations. Future work using endogenous systems, including cells derived from patients harboring the mutations or CRISPR knock-in strategies to generate heterozygous mutant cell lines, would offer more direct and detailed insights into their functions.

It is tempting to speculate that dysregulation of GPCR signaling could be one important molecular pathway that contributes to the neuronal pathologies stemming from loss of RBM12. More than a third of all known GPCRs are expressed in the brain, where they bind to neurotransmitters and play essential roles in synaptic and structural plasticity (46–48). Dysregulation of GPCR activity in the brain also contributes to the pathophysiology of several neurological and neuropsychiatric disorders (49–51). Similarly, cAMP is a critical second messenger that mediates all important aspects of neuronal function, including development, excitability, and plasticity (52). While most of this work is centered around the prototypical β2-AR, we report that RBM12 function is required for normal cAMP production downstream of other Gαs-coupled receptors with established roles in the nervous system (dopamine 1 and adenosine receptors, Fig. 1, *D* and *E*) (14, 53). This finding is perhaps not surprising given that all stimulatory GPCRs converge on the same components of the cAMP–PKA pathway, many of which are dysregulated in the absence of RBM12 (Fig. 7*B*). As a result, the neuronal GPCR-driven transcriptional responses are altered when *RBM12* is knocked down. Specifically, the entire repertoire of targets, many of which orchestrate processes essential for neuronal differentiation, gene reprogramming, and memory and learning, shows a trend towards hyperactivation in depleted neurons (Fig. 6*A*). Moreover, more than 100 genes are induced in response to receptor stimulation only in the knockdown. Most notable among this set are *ARC* and *BDNF*, two factors with crucial roles in synaptic function, plasticity, and learning (Table S1) (54, 55). At the same time, we cannot rule out the possibility that RBM12 impacts processes in the brain through additional mechanisms. In fact, we identify extensive reprogramming of RBM12 knockdown neurons beyond expression of cAMP pathway effectors, as the set of altered GO categories includes neuron differentiation, synapse organization, and neurogenesis (Fig. 7*A* and Table S2). It remains to be determined how all these changes collectively impact neuronal function and to what extent any of the alterations are driven specifically by dysregulation of the receptor pathway. Further, a different *RBM12* mutation has been implicated in the aberrant development of the mouse forebrain and midbrain (12). Therefore, investigation of the neurodevelopmental consequences of RBM12 depletion would likewise be warranted. Lastly, PDE1C, one of the two PDE isoforms depleted in neurons lacking RBM12, exhibits high affinity for both cAMP and cGMP (56). While we do not detect differences in basal cGMP across the mutant cell lines (Fig. S6*C*), it is possible that cGMP accumulation is subject to RBM12-dependent regulation and this aspect should likewise be considered.

The cAMP/PKA cascade has been implicated in neuropsychiatric disorders in the past, supporting the requirement for tightly regulated cAMP signaling for proper neuronal function. A study on postmortem brains of patients with bipolar affective disorder demonstrated elevated levels of the PKAcat subunit Cα in temporal and frontal cortices compared to matched normal brains (57, 58). A different report on patient-derived platelet cells found that the catalytic subunit of cAMP-dependent protein kinase was significantly upregulated in untreated depressed and manic patients with bipolar disorder compared with untreated euthymic patients with bipolar disorder and healthy subjects (59). In the context of schizophrenia, cAMP/PKA signaling has been found to be both reduced and hyperactive. For example, the PKA regulatory subunits, RI and RII, were significantly reduced in platelets from schizophrenic patients in one report (60), and several adenylyl cyclase isoforms were downregulated in patient fibroblasts reprogrammed into iPSC neurons in another (61). While this manuscript was under preparation, a study reported similar findings to ours with respect to the tentative molecular pathways dysregulated in loss-of-function mutants of another risk factor associated with neurodevelopmental defects and schizophrenia. Specifically, the authors found that heterozygous mutations in the histone methyltransferase SET domain-containing protein 1 A (*SETD1A*) led to transcriptional and signaling signatures supporting hyperactivation of the cAMP pathway through upregulation of adenylyl cyclases and downregulation of PDEs (62). This in turn resulted in increased dendritic branching and length and altered network activity in hiPSC-derived glutamatergic neurons (62). Therefore, the cAMP–PKA pathway appears to be a common point of convergence downstream of different risk factors for neuropsychiatric disorders and could present a therapeutic target in certain genetic contexts.

In summary, this study identifies a previously unappreciated role for RBM12 in the context of the GPCR–PKA–cAMP pathway. Because the regulation is conserved across multiple receptors and in two different cell models, it is likely of broad

relevance and should be explored further as a tentative molecular mechanism underlying the functions of RBM12 in brain physiology and pathophysiology.

## Experimental procedures

### Chemicals

(–)-Isoproterenol hydrochloride was purchased from Sigma-Aldrich (Cat. #I6504), dissolved in 100 mM ascorbic acid to 10 mM stock, and used at indicated concentrations. Alprenolol hydrochloride was purchased from Sigma-Aldrich (Cat. #A0360000), dissolved in dimethyl sulfoxide (DMSO) to 10 mM stock, and used at 10 μM final concentration. Norepinephrine was purchased from Sigma (Cat. #A7257), dissolved in 100 mM ascorbic acid to 10 mM stock, and used at 10 μM final concentration. (–) Epinephrine was purchased from Sigma (Cat. #E4250), dissolved in 100 mM ascorbic acid to 10 mM stock, and used at 10 μM final concentration. Salbutamol was purchased from Cayman Chemical Company (Cat. #21003), dissolved in DMSO to 10 mM stock, and used at 10 μM final concentration. Formoterol fumarate dihydrate was purchased from Sigma Aldrich (Cat. #F9552), dissolved in DMSO to 10 mM stock, and used at 50 nM final concentration. Terbutaline hemisulfate salt was purchased from Sigma-Aldrich (Cat. #T2528), dissolved in water to 10 mM stock, and used at 10 μM final concentration. 5′-(N-Ethyl Carboxamide) adenosine was purchased from Sigma-Aldrich (Cat. #119140), dissolved in DMSO to 10 mM stock, and used at 10 μM final concentration. SKF-1297 hydrobromide was purchased from Tocris (Cat. #1447), dissolved in DMSO to 10 mM stock, and used at 10 nM final concentration. ICI-118,551 hydrochloride was purchased from Sigma-Aldrich (Cat. #I127), dissolved in water to 10 mM stock, and used at 10 μM final concentration. Dopamine hydrochloride was purchased from Sigma Aldrich (Cat. #H8502), dissolved in 100 mM ascorbic acid to 10 mM stock, and used at 10 μM final concentration. DAMGO was purchased from Tocris (Cat. #1171), dissolved in DMSO to 10 mM stock, and used at 10 μM final concentration. 8-CPT-cAMP was purchased from Abcam (Cat. #ab120424), dissolved in water to 150 mM stock, and used at 150 μM final concentration for the RT-qPCR experiment. Forskolin was purchased from Sigma-Aldrich (Cat. #F6886), dissolved in DMSO to 10 mM stock, and used at 1 μM or 10 μM final concentration. Rolipram was purchased from Tocris (Cat. #0905), dissolved in ethanol to 10 mM stock, and used at 10 μM final concentration. Shield-1 ligand for stabilization of DD-tagged proteins was purchased from Aobious (Cat. #AOB1848), dissolved in ethanol to 1 mM stock, and added to the cell medium to 1 μM final concentration. D-luciferin sodium salt (Cat. #LUCNA) and coelenterazine (Cat. #CZ) were purchased from GoldBio and resuspended to 100 mM in 10 mM Hepes buffer and 10 mM in ethanol, respectively, and stored protected from light. Dyngo-4a was purchased from Abcam (Cat. #ab120689), dissolved in DMSO to 30 mM stock, and added to cells grown in serum-free medium to a final concentration of 30 μM for 20 min prior to drug treatment.

### Constructs and siRNA

The previously described lentiCRISPRv2 vector for CRISPR KO gRNA expression was a gift from Feng Zhang (Addgene, Cat. #52961). gRNAs were cloned by annealing complementary oligonucleotides purchased from IDT (Table S3) and ligation into BsmBI-digested lentiCRISPRv2 as described previously (63, 64). The parental vector for CRISPRi gRNA expression under a U6 promoter (pU6-gRNA-EF1alpha-puro-T2A-BFP) was a gift from Jonathan Weissman (Addgene, Cat. #60955) (65, 66). gRNAs were cloned by annealing complementary oligonucleotides purchased from IDT (Table S3) and ligation into BstXI/BlpI-digested pU6-gRNA-EF1alpha-puro-T2A-BFP backbone as described previously (8).

The plasmid encoding the cAMP luminescence biosensor with *Renilla* luciferase (pSF-CMV-GloSensor20F-IRES-Rluc, pGLO) and CMV promoter-driven FLAG-tagged-β2-AR were described previously (8, 13, 17). *DRD1*-Tango was a gift from Bryan Roth (University of North Carolina) (Addgene, Cat. #66268). pcDNA 3.1-D2R, pcDNA 3.1-delta opioid receptor, and pcDNA 3.1-SSF-mu opioid receptor were a gift from Mark von Zastrow (University of California) and transfected for 24 h in HEK293 cells seeded on 6-well plates. Plasmids encoding TagBFP-PKAcat and ExRai-AKAR2 sensor were a gift from Jin Zhang (University of California) and transfected for 24 h in HEK293 cells seeded on 6-well plates (TagBFP-PKAcat) or 35 mm imaging dishes (ExRai-AKAR2). The low expression β2-AR plasmid was generated by amplifying a genomic region that included the ∼1 kb sequence upstream of the *ADRB2* ORF, which contains the annotated 5′ UTR and promoter, and the gene coding sequence. β2-AR and CMV-β2-AR plasmids were transfected for 48 h in HEK293 cells seeded on 6-well plates.

To generate the EGFP-RBM12 plasmid, the WT human *RBM12* ORF sequence was PCR amplified from a plasmid encoding human *RBM12* in pDONR221 (DNASU, Cat. #HsCD00042134) and inserted into SacI-digested pEGFP-C1 backbone by In-Fusion cloning with an added stop codon. EGFP-c.2377G>T-RBM12 and EGFP-c.2532delT-RBM12 were generated using QuikChange site-directed mutagenesis of the WT EGFP-RBM12. To generate lentiviral plasmids encoding the WT and mutated EGFP-RBM12 constructs, the *RBM12* sequence was PCR amplified and inserted into XbaI-digested lentiviral FHUGW-EGFP (gift from Mark von Zastrow, University of California) backbone by In-Fusion cloning.

A lentiviral plasmid encoding a transcriptional reporter for CREB activity (FHUGW-CRE-DD-zsGreen) was previously described (8). To generate a CREB activity reporter driving the production of the tdTomato fluorescent protein (FHUGW-CRE-DD-tdTomato), a sequence encoding the tdTomato fluorescent protein was amplified from a pBa-KIF5C 559-tdTomato-FKBP plasmid (Addgene, Cat. #64211) and inserted into the linearized FHUGW-CRE-DD-zsGreen plasmid by In-Fusion cloning.

Synthetic RNA duplexes (RBM12_8, Cat. #1027417; AllStar Negative Control, Cat. #1027281) were obtained from the validated HP GenomeWide siRNA collection (Qiagen) and

transfected for 72 h using Lipofectamine-RNAiMax (Invitrogen, Cat. #13778150) according to the manufacturer's instructions.

### *Cell culture*

HEK293 (from Mark von Zastrow, University of California) and HEK293T (TakaraBio, Cat. #632180) cells were grown at 37 °C/5% $CO_2$ in Dulbecco's Modified Eagle Medium (DMEM, 4.5 g/L glucose and L-glutamine, no sodium pyruvate) (Thermo Fisher Scientific, Cat. #11965118) supplemented with 10% fetal bovine serum (Sigma Aldrich, Cat. #F2442).

hiPSCs engineered to express *NGN2* under a doxycycline-inducible system in the AAVS1 safe harbor locus were described previously (32). hiPSCs stably expressing FLAG-β2-AR under ubiquitin promoter were generated by lentiviral transduction, labeling with M1-Alexa-647 and fluorescent cell sorting. We specifically selected clones that express low levels of FLAG-β2-AR. hiPSCs were cultured in Essential 8 Medium (Thermo Fisher Scientific, Cat. #A1517001) on plates coated with Growth Factor Reduced, Phenol Red-Free, LDEV-Free Matrigel Basement Membrane Matrix (Corning, Cat. #356231) diluted in KO DMEM to 0.1 mg/ml concentration (Thermo Fisher Scientific, Cat. #10829-018). Essential 8 Medium was replaced every 2 days. For lentiviral infection of hiPSCs, cells were infected for 3 to 4 days before neuronal differentiation.

### *Lentivirus production*

HEK293T cells were transfected with lentiviral constructs (WT or mutated EGFP-RBM12, CREB reporter, or CRISPRi gRNA) and standard packaging vectors (VSVG and psPAX2) using Lipofectamine-2000 (Invitrogen, Cat. #11668027) following recommended protocols. Supernatant was harvested 72 h after transfection and filtered through a 0.45 μm SFCA filter. The harvested virus was either used on the same day or concentrated and snap-frozen before use.

### *HEK293 CRISPR KO and CRISPRi*

RBM12 CRISPR KO HEK293 clones were generated by transfecting WT cells with two independent gRNAs (Table S3) using Lipofectamine-2000 transfection reagent (Thermo Fisher Scientific, Cat. #11668027) following recommended protocols. Cells were selected with 1 μg/ml puromycin for 2 days, then recovered and plated as single colonies. Individual clones were expanded for at least 3 weeks and tested for successful editing using Sanger sequencing of genomic DNA. Parental WT cells were grown in parallel and serve as experimentally matched control. Sanger sequencing of the RBM12 KO cells shows the occurrence of insertion and deletion events that lead to a frameshift and a premature stop in both lines (Fig. S2*A*). Using RT-qPCR analysis, we found that *RBM12* RNA levels were unaffected in KO 1 but reduced in KO 2 (Fig. S2*B*).

WT and RBM12 KO HEK293 cells stably expressing FLAG-tagged β2-AR were generated by transfecting cells seeded on 6-well plate with the FLAG-β2-AR plasmid for 72 h prior to selection of stable cells using 100 μg/ml G418 sulfate (Genesee Scientific, Cat. #25-538).

For CRISPRi-mediated knockdown, control gRNA (NTC) and *RBM12*-targeting gRNA (RBM12_783) were cloned into the parental vector for gRNA expression under a U6 promoter (pU6-gRNA-EF1alpha-puro-T2A-BFP) at the BlpI/BstXI sites. Previously described HEK293 cells stably expressing dCas9-BFP-KRAB (8) were seeded on 6-well dishes at ∼30% confluence and transduced with lentiviral supernatant containing the gRNAs of interest with or without the fluorescent CREB reporter. Forty eight hours after transduction with the gRNAs, cells were selected with 1 μg/ml puromycin for 2 days, then recovered and expanded for 3 days in regular medium without antibiotic. For rescue experiments in HEK293, equal volumes of viral supernatant containing WT or mutated RBM12 lentiviral constructs were transduced together with the gRNAs on the first day. To generate stable CRISPRi-mediated *RBM12* knockdown hiPSCs, cells were transduced with lentiviral supernatant containing NTC or *RBM12*-targeting gRNA for 2 days followed by fluorescent cell sorting of gRNA-positive cells. For rescue experiments in neurons, NTC or *RBM12* gRNA-transduced hiPSCs were transduced with lentiviral supernatant containing EGFP vector, EGFP-WT, EGFP-c.2377G>T, or EGFP-c.2532delT RBM12 for 2 days and sorted based on EGFP expression prior to differentiation into neurons.

### *iNeuron differentiation*

iNeurons were generated by hiPSC differentiation for 14 days as described previously (32). Briefly, hiPSCs were lifted using Accutase and centrifuged. Pelleted cells were resuspended in N2 pre-differentiation medium containing the following: Knockout DMEM/F12 (Thermo Fisher Scientific, Cat. #12660-012) as the base, 1× MEM non-essential amino acids (Thermo Fisher Scientific, Cat. #11140-050), 1× N2 supplement (Thermo Fisher Scientific, Cat. #17502-048), 10 ng/ml NT-3 (PeproTech, Cat. #450-03), 10 ng/ml BDNF (PeproTech, Cat. #450-02), 1 μg/ml mouse Laminin (Thermo Fisher Scientific, Cat. #23017-015), 10 nM Y-27632 dihydrochloride ROCK inhibitor (Tocris, Cat. #125410), and 2 μg/ml doxycycline hydrochloride (Sigma-Aldrich, Cat. #D3447-500 MG) to induce expression of *NGN2*. iPSCs were counted and plated at $5 \times 10^5$ cells per Matrigel-coated well of a 6-well plate in N2 pre-differentiation medium with 1 μg/ml doxycycline hydrochloride for 3 days. Afterward, predifferentiated cells were lifted and centrifuged as above, and the cell pellet was resuspended in Classic Neuronal Medium containing the following: half DMEM/F12 (Thermo Fisher Scientific, Cat. #11320-033) and half Neurobasal-A (Thermo Fisher Scientific, Cat. #10888-022) as the base, 1× MEM non-essential amino acids, 0.5× GlutaMAX supplement (Thermo Fisher Scientific, Cat. #35050-061), 0.5× N2 supplement (Thermo Fisher Scientific, Cat. #17502048), 0.5× B27 supplement (Thermo Fisher Scientific, Cat. #17504-044), 10 ng/ml NT-3 (PeproTech, Cat. #450-03), 10 ng/ml BDNF (PeproTech, Cat. #450-02), 1 μg/ml mouse Laminin (Thermo Fisher Scientific, Cat. #23017015), and 1 μg/ml doxycycline hydrochloride (Sigma-Aldrich, Cat.

#D3447). Predifferentiated cells were counted and plated at $3.5 \times 10^5$ cells per well of a BioCoat Poly-D-Lysine 12-well plate (Corning, Cat. #356470) in Classic Neuronal Medium or at $7 \times 10^6$ cells per well of a BioCoat Poly-D-Lysine 6-well plate (Corning, Cat. #356469). After 7 days, half of the medium was removed and an equal volume of fresh Classic Neuronal Medium without doxycycline was added. After 14 days, half of the medium was removed and twice the volume of fresh Classic Neuronal Medium without doxycycline was added. For EGFP-RBM12 live-cell imaging experiments, iPSCs were counted and plated at $2 \times 10^5$ cells per Matrigel-coated well of 35 mm imaging dish (Matsunami, Cat. #D1113OH) in N2 predifferentiation medium for 3 days, followed by media change using the Classic Neuronal Medium to induce differentiation.

### *RT-qPCR analysis of target gene expression*

For RT-qPCR experiments, cells were left untreated or treated with the indicated dose of drug for 1 h in DMEM + 10% FBS prior to RNA extraction. For Dyngo-4a experiments, cells were pretreated with DMSO or 30 μM Dyngo-4a in serum-free DMEM for 20 min prior to treatment with 1 μM Iso for 1 h. Total RNA was extracted from the samples using the Zymo Quick-RNA Miniprep Kit (Genesee, Cat. #11–327) or Qiagen RNeasy Mini Kit (Qiagen, Cat. #74106). Reverse transcription was carried out using iScript RT supermix (Bio-Rad, Cat. #1708841) or Superscript II Reverse Transcriptase (Thermo Fisher Scientific, Cat. #180644022) following recommended manufacturer protocols. The resulting complementary DNA was used as input for RT-qPCR using CFX-384 Touch Real-Time PCR System (Bio-Rad), Power SYBR Green PCR MasterMix (Thermo Fisher Scientific, Cat. #4367659), and the appropriate primers (Table S4). All transcript levels were normalized to the levels of the housekeeping gene *GAPDH*.

### *cAMP production*

For pGLO sensor real-time measurement of cAMP production, cells seeded on 6-well plates were transfected with pGLO-20 F/Rluc alone or with the indicated receptor plasmid (D1R, D2R, mu OR, delta OR) for 24 h using Lipofectamine 2000 transfection reagent following manufacturer's protocols. On the day of the experiment, cells were replated onto a 96-well plate in medium supplemented with 160 μM D-luciferin and incubated for 40 min prior to conducting the assay. To measure cAMP production in response to Gαs-receptor activation, Hamamatsu FDSS/μCell with liquid handling was equilibrated at 37 °C and used to dispense the drugs (100 nM isoproterenol for β2-AR, 10 μM 5′-(N-Ethyl Carboxamide) adenosine for A1/2R, 10 nM SKF-81297 for D1R) and simultaneously image cAMP-driven luciferase activity in real time. All experimental cAMP measurements (firefly luciferase time course data) were normalized to the *Renilla* luciferase signal (expression control), and the averaged normalized maximum values from the control samples for each tested batch was set to 100%, and all values are shown as % of this mean. D1R expression in transfected cells incubated with anti-HA-Alexa-488 (Thermo Fisher Scientific, Cat. #A-21287) for 1 h on ice was measured by flow cytometry using BD FACS Canto2. To measure Gαi-receptor responses, cells were either treated with 1 μM forskolin + vehicle (DMSO), 1 μM forskolin + 10 μM DOPA + 10 μM ICI-118,551 (D2R), or 1 μM forskolin + 10 μM DAMGO (μOR and ΔOR). At the end of the time course, cells were lysed in stop buffer (5 mM Hepes, 2% glycerol, 1 mM EDTA, 400 μM DTT, 0.2% Triton) supplemented with 2 μM coelenterazine. All experimental cAMP measurements (firefly luciferase time course data) were normalized to the *Renilla* luciferase signal (expression control), and the inhibition of forskolin response (GPCR drug/forskolin) was calculated from each cell line. The averaged forskolin inhibition in the control samples for each tested batch was set to 100%, and all values are shown as % of this mean.

For the cADDis sensor, neurons were transduced with the BacMam sensor according to manufacturer's instructions for 24 h. On the day of the experiment, neurons were lifted with papain (Sigma-Aldrich, Cat. #P4762) and 100,000 cells were resuspended in 100 μl Hanks' Balanced Salt Solution (Thermo Fisher Scientific, Cat. #14175-095) supplemented with 30 mM Hepes (Sigma Aldrich, Cat. #H0887) per well prior to drug addition and fluorescence reading using the TECAN Spark plate reader. For ELISA experiments, Cyclic AMP ELISA Kit (Cayman Chemical, Cat. #581001) was used according to manufacturers' instructions and read using the TECAN Spark plate reader. All values were normalized to total protein amounts.

### *Receptor trafficking*

WT and RBM12 KO cells stably expressing FLAG-tagged β2-AR were seeded on 12-well plates. To induce β2-AR internalization, cells were treated with 1 μM isoproterenol for 20 min. Then, cells were put on ice to stop trafficking, lifted, and labeled with Alexa 647–conjugated M1 antibody. To induce β2-AR recycling, cells were first treated with 1 μM isoproterenol for 20 min and then 10 μM alprenolol for 40 min. Untreated cells served as a proxy for total β2-AR cell surface expression. Flow cytometry analysis was carried out using a BD FACS Canto2 instrument, and Alexa-647 mean signal of the gated singlet population was used as a proxy for total number of surface receptors. Calculations were carried out for each cell line as follows: % internalized receptors = 100%-(total # surface receptors after 20 min isoproterenol)/(total # surface receptors pre-drug) × 100%; % recycled receptors = (total # surface receptors 40 min after alprenolol - total # surface receptors after 20 min iso)/(total initial # surface receptors - total # surface receptors after 20 min iso)] x 100%. The mean Alexa-647 WT values for the batch were set to 100%, and all values are shown as % of this mean.

### *Flow cytometry–based experiments with pCRE-DD-zsGreen1 and pCRE-DD-tdTomato*

For fluorescent CREB reporter experiments, cells were seeded on 6-well plates and transduced with lentiviral supernatant containing the fluorescent CREB reporter (8). Cells were

maintained for 5 to 7 days before experiments. On the experiment day, cells were treated for 4 h with 1 μM Shield-1 ligand alone (basal) or with 1 μM Shield-1 ligand and one of the following: 1 μM isoproterenol, 10 μM epinephrine, 10 μM norepinephrine, 50 nM salbuterol, 10 μM terbutaline, 10 μM formoterol prior to fluorescence reading using the BD FACS Canto2 flow cytometry instrument. For pCRE-DD-tdTomato experiments, cells were treated with 1 μM Shield-1 ligand alone (basal) or with 1 μM Shield-1 ligand and 1 μM isoproterenol for 6 h. We used a BD LSRFortessa flow cytometry instrument and gated for gRNA-expressing (BFP+) and RBM12 construct–expressing (GFP+) singlets. From these measurements, the fold change (induced/basal) mean of the NTC gRNA + empty vector cells was averaged and set to 1, and the PE (tdTomato) mean for all other samples was normalized to this value (expressed as fold of mean NTC value).

### *Microscopy*

HEK293 cells were seeded on poly-L-lysine– (Sigma, Cat. #P8920) coated coverslips in 12-well plates. iNeurons were plated on poly-D-lysine-coated plates. Cells were fixed in 3.7% formaldehyde/PBS or 4% paraformaldehyde/PBS for 20 min. Next, cells were stained using 1:100 to 1:500 anti-RBM12 primary antibody (Santa Cruz Biotechnology, Cat. #sc-514258) for 1 to 2 h and 1:1000 Alexa fluor secondary antibodies for 30 min dissolved in 3% Bovine serum albumin/0.1% Triton-X/PBS blocking and permeabilizing solution. Lastly, cells were incubated with 1:5000 DAPI (1 mg/ml stock) in PBS for 5 min.

For PKA activity measurements, HEK293 cells seeded on 35-mm imaging dishes (Matsunami, Cat. #D1113OH) were transfected with the ExRai-AKAR2 plasmid for 24 h. On the day of the experiment, the medium was changed to DMEM (4.5 g/L glucose, no glutamine, no sodium pyruvate, no phenol red) (Thermo Fisher Scientific, Cat. #31053028) supplemented with 30 mM Hepes (Sigma Aldrich, Cat. #H0887), and cells were treated with the indicated drug concentration. Regions of interest were drawn around the cell to measure mean fluorescence values in FIJI. PKA activity was measured by calculating $\Delta F/F = (F_t - F_0)/F_0$, with $F_t$ representing the GFP fluorescence at a specific time point and $F_0$ representing the initial GFP fluorescence.

Live and fixed cell imaging was performed on the Andor Dragonfly spinning disk microscope using the 40×/1.3 HC PL APO CS2 oil, WD: 0.24 mm objective lens (Leica, Cat. #11506358), 405-nm and 488-nm diode lasers (Andor), and 450/50 and 525/50 excitation/emission filters. The Andor iXon 888 Life EMCCD camera with 1024x1024 pixel was used with 200 EM gain. Images were collected with Andor Fusion Software (https://andor.oxinst.com/downloads/view/fusion-release-2.3). Live cell imaging was carried out in a 37 °C chamber (Okolab).

### *Protein extraction and western blot*

Cells were lysed with RIPA buffer (Sigma Aldrich, Cat. #R0278) containing protease inhibitors cocktail (Sigma-Aldrich, Cat. #P8340) and 0.1 μM PMSF (Sigma-Aldrich, Cat. #P7626). Lysates were then transferred to microcentrifuge tubes and spun for 5 min at 14,000 r.p.m. at 4 °C. The supernatant was used for Western blot experiments. Protein concentration was determined by Pierce BSA Protein Assay Kit (Thermo Fisher Scientific, Cat. #23225). Protein samples were prepared for Western blot analysis by adding 4× sample buffer (Bio-Rad, Cat. #1610747) and 1 mM DTT (Sigma, Cat. #D0632). Samples were loaded onto a 4 to 15% MINI-PROTEAN TGX Stain-Free gels (Bio-Rad, Cat. #4568083) and transferred to nitrocellulose membrane for 1.5-3 h at 100 V in 4 °C. Afterward, membranes were blocked with 5% milk in Tris-buffered saline with 0.1% Tween-20 detergent (TBST) for 30 min and incubated with primary antibodies/TBST against proteins of interest: anti-RBM12 (Santa Cruz Biotechnology, Cat. #sc-514258), anti-PKA alpha polyclonal antibody (Thermo Fisher Scientific, Cat. #PA5-17626), and anti-beta-actin (Santa Cruz Biotechnology, Cat. #sc-69879). The following day, membranes were washed, incubated in the corresponding horseradish peroxidase-conjugated secondary antibodies/TBST, and developed using Classico Western horseradish peroxidase substrate (Millipore Sigma, Cat. #WBLUC0100). Alternatively, membranes were washed, incubated with secondary antibody 1:10,000 diluted donkey anti-mouse-680 (LICOR Biosciences, Cat. #926-68072) and 1:10,000 diluted donkey anti-rabbit-800 (LICOR Biosciences, Cat. #926-32213) in LICOR blocking buffer (LICOR Biosciences, Cat. #927-40000), and visualized using the Odyssey imager system (LICOR). Bands were analyzed using densitometry analysis in ImageJ (https://imagej.nih.gov/ij/download.html) or the LICOR (https://www.licor.com/bio/image-studio/) software. Scans of uncropped and unprocessed blots are provided.

### *RNA-seq library preparation and analysis*

RNA was extracted using the RNeasy Plus Mini Kit (Qiagen, Cat. #74106). One microgram of RNA and 500 ng RNA were used as input for sequencing libraries generation for HEK293 and neurons, respectively, and isolated using NEBNext Poly(A) mRNA magnetic isolation module (New England Biolabs, Cat. #E7490). HEK293 libraries were generated using NEBNext Ultra RNA Library Prep Kit for Illumina (New England Biolabs, Cat. #E7770) or NEBNext Ultra II Directional RNA Library Prep Kit for Illumina (#E7760), and NEBNext Multiplex Oligos for Illumina (New England Biolabs, Cat. #E7735S) according to the manufacturer's instructions. Libraries were sequenced on NovaSeq 6000. Raw sequencing reads were analyzed using FastQC for quality control (http://www.bioinformatics.babraham.ac.uk/projects/fastqc). Reads were aligned to the *Homo sapiens* GRCh38 assembly using STAR aligner (67). Raw read counts for each sample were obtained using featureCounts (68). Only genes with more than five counts in a minimum of four samples were included in the downstream analysis. Normalized counts and differential gene expression analysis was carried out in R using the DESeq2 pipeline (69).

For the neuronal RNA-seq analysis in moderate β2-AR–overexpressing neurons, we independently identified β2-AR

target sets by differential expression analysis between untreated and isoproterenol-treated neurons in NTC and *RBM12* knockdown using DESeq2. Using a stringent statistical cut-off of gene $p_{adj} < 5.0 \times 10^{-2}$ (Wald test) and $\log_2$ fold change ≥ 0.5, we obtained 208 and 576 targets from NTC and *RBM12* knockdown neurons, respectively. Of these, a total of 669 genes were unique and constituted the set of β2-AR–dependent transcriptional neuronal targets. For differential expression analysis between NTC and *RBM12* knockdown neurons, we applied a statistical cutoff of $p_{adj} < 5.0 \times 10^{-2}$ (Wald test) and $\log_2$ fold change ≥ 0.1 or ≤ 0.1. GO analysis was performed using the two unranked list method in GOrilla (30) using $p_{adj}$ cutoff of $< 5.0 \times 10^{-2}$ (Fisher's exact test). For RNA-seq analysis in neurons derived from the parental iPSC, we performed differential expression analysis between untreated and isoproterenol-treated RBM12 knockdown neurons using DESeq2 and performed simple linear regression analysis of the shared targets between the parental and β2-AR–overexpressing neurons.

### *Statistical analysis and reproducibility*

All data are shown as mean ± SD. Statistical analyses to determine significance were performed using DESeq2 with Wald test for RNA-seq experiments and Prism v.8 (GraphPad) for unpaired two-sided Student *t* test, one-, or two-way ANOVA ($\alpha$, 0.05) for all other experiments. Asterisks are used to denote statistical significance (* = $p \le 0.05$, ** $p \le 0.01$, *** $p \le 0.001$, **** $p \le 0.0001$).

## Data availability

Raw reads and normalized counts from the RNA-seq data generated in this study have been deposited on the Gene Expression Omnibus (GSE219195 and GSE229254).

*Supporting information*—This article contains supporting information.

*Acknowledgments*—We thank members of the Tsvetanova lab for valuable discussion and critical feedback on the manuscript. We thank Dr Martin Kampmann (University of California, San Francisco, CA) for generously providing the human iPSC line WTc11. We acknowledge the Duke Cancer Institute Flow Cytometry Shared Resource and the Duke University Light Microscopy Core Facility. Dr Jin Zhang (University of California, San Diego, CA) provided the TagBFP-PKAcat and ExRai-AKAR2 constructs. Dr Mark von Zastrow (University of California, San Francisco, CA) provided the pcDNA 3.1-D2R, pcDNA 3.1-Δ- and μ-opioid receptors, and FHUGW-EGFP constructs. Figures 4*D*, 5*A* and 7*E* were created using BioRender.

*Author contributions*—K. M. S. and N. G. T. conceptualization; K. M. S., A. G., and N. G. T. investigation; K. M. S., A. G., and N. G. T. formal analysis; K. M. S. and N. G. T. funding acquisition; K. M. S., A. G., and N. G. T. methodology; N. G. T. supervision; K. M. S., A. G., and N. G. T. writing–review and editing.

*Funding and additional information*—This work was supported by the National Institutes of Health (R35GM142640 to N. G. T.), the American Association of University Women (2021 International Fellowship to K. M. S.), and the American Heart Association (Pre-Doctoral Fellowship #898739 to K. M. S.). The content is solely the responsibility of the authors and does not necessarily represent the official views of the National Institutes of Health.

*Conflicts of interest*—The authors declare that they have no conflicts of interests with the contents of this article.

*Abbreviations*—The abbreviations used are: β2-AR, beta-2-adrenergic receptor; BDNF, brain-derived neurotrophic factor; CREB, cAMP response-element binding protein; CRISPRi, CRISPR interference; DMEM, Dulbecco's modified Eagle's medium; DMSO, dimethyl sulfoxide; GO, gene ontology; GPCR, G protein–coupled receptor; gRNA, guide RNA; hiPSC, human neurons derived from induced pluripotent stem cell; NGN2, Neurogenin 2; NTC, non-targeting control; PDE, phosphodiesterase; PKAcat, PKA catalytic; RBM 12, RNA-binding motif 12; RRM, RNA-recognition motif; RT-qPCR, reverse transcription/quantitative PCR; TBST, Tris-buffered saline with 0.1% Tween-20 detergent.

## References

1. Hauser, A. S., Attwood, M. M., Rask-Andersen, M., Schiöth, H. B., and Gloriam, D. E. (2017) Trends in GPCR drug discovery: new agents, targets and indications. *Nat. Rev. Drug Discov.* **16**, 829–842
2. Moore, C. A., Milano, S. K., and Benovic, J. L. (2007) Regulation of receptor trafficking by GRKs and arrestins. *Annu. Rev. Physiol.* **69**, 451–482
3. Weis, W. I., and Kobilka, B. K. (2018) The molecular basis of G protein–coupled receptor activation. *Annu. Rev. Biochem.* **87**, 897–919
4. Plouffe, B., Thomsen, A. R. B., and Irannejad, R. (2020) Emerging role of compartmentalized G protein-coupled receptor signaling in the cardiovascular field. *ACS Pharmacol. Transl. Sci.* **3**, 221–236
5. Jong, Y. I., Harmon, S. K., and O'Malley, K. L. (2018) GPCR signalling from within the cell. *Br. J. Pharmacol.* **175**, 4026–4035
6. Crilly, S. E., and Puthenveedu, M. A. (2021) Compartmentalized GPCR signaling from intracellular membranes. *J. Membr. Biol.* **254**, 259–271
7. Chaturvedi, M., Schilling, J., Beautrait, A., Bouvier, M., Benovic, J. L., and Shukla, A. K. (2018) Emerging paradigm of intracellular targeting of G protein-coupled receptors. *Trends Biochem. Sci.* **43**, 533–546
8. Semesta, K. M., Tian, R., Kampmann, M., von Zastrow, M., and Tsvetanova, N. G. (2020) A high-throughput CRISPR interference screen for dissecting functional regulators of GPCR/cAMP signaling. *PLoS Genet.* **16**, e1009103. https://doi.org/10.1371/journal.pgen.1009103
9. Wakabayashi, A., Kihiu, M., Sharma, M., Thrasher, A. J., Saari, M. S., Quesnel-Vallières, M., *et al.* (2022) Identification and characterization of RBM12 as a novel regulator of fetal hemoglobin expression. *Blood Adv.* https://doi.org/10.1182/bloodadvances.2022007904
10. Consortium, T. U. (2020) UniProt: the universal protein knowledgebase in 2021. *Nucleic Acids Res.* **49**, D480–D489
11. Steinberg, S., Gudmundsdottir, S., Sveinbjornsson, G., Suvisaari, J., Paunio, T., Torniainen-Holm, M., *et al.* (2017) Truncating mutations in RBM12 are associated with psychosis. *Nat. Genet.* **49**, 1251–1254
12. Sun, M., Mondal, K., Patel, V., Horner, V. L., Long, A. B., Cutler, D. J., *et al.* (2012) Multiplex chromosomal exome sequencing accelerates identification of ENU-induced mutations in the mouse. *G3 (Bethesda)* **2**, 143–150
13. Wigdal, S. S., Anderson, J. L., Vidugiris, G. J., Shultz, J., Wood, K. V., and Fan, F. (2008) A novel bioluminescent protease assay using engineered firefly luciferase. *Curr. Chem. Genomics* **2**, 16–28
14. Beaulieu, J. M., and Gainetdinov, R. R. (2011) The physiology, signaling, and pharmacology of dopamine receptors. *Pharmacol. Rev.* **63**, 182–217
15. Valentino, R. J., and Volkow, N. D. (2018) Untangling the complexity of opioid receptor function. *Neuropsychopharmacology* **43**, 2514–2520

16. Zhang, J.-F., Liu, B., Hong, I., Mo, A., Roth, R. H., Tenner, B., *et al.* (2021) An ultrasensitive biosensor for high-resolution kinase activity imaging in awake mice. *Nat. Chem. Biol.* **17**, 39–46
17. Tsvetanova, N. G., and von Zastrow, M. (2014) Spatial encoding of cyclic AMP signaling specificity by GPCR endocytosis. *Nat. Chem. Biol.* **10**, 1061–1065
18. Slotkin, T. A., Lappi, S. E., and Seidler, F. J. (1995) β-Adrenergic control of c-fos expression in fetal and neonatal rat tissues: relationship to cell differentiation and teratogenesis. *Toxicol. Appl. Pharmacol.* **133**, 188–195
19. Larson, M. H., Gilbert, L. A., Wang, X., Lim, W. A., Weissman, J. S., and Qi, L. S. (2013) CRISPR interference (CRISPRi) for sequence-specific control of gene expression. *Nat. Protoc.* **8**, 2180–2196
20. Zhu, J., Mix, E., and Winblad, B. (2001) The antidepressant and antiinflammatory effects of rolipram in the central nervous system. *CNS Drug Rev.* **7**, 387–398
21. Peng, G. E., Pessino, V., Huang, B., and von Zastrow, M. (2021) Spatial decoding of endosomal cAMP signals by a metastable cytoplasmic PKA network. *Nat. Chem. Biol.* **17**, 558–566
22. Bowman, S. L., Shiwarski, D. J., and Puthenveedu, M. A. (2016) Distinct G protein–coupled receptor recycling pathways allow spatial control of downstream G protein signaling. *J. Cell Biol.* **214**, 797–806
23. McCluskey, A., Daniel, J. A., Hadzic, G., Chau, N., Clayton, E. L., Mariana, A., *et al.* (2013) Building a better dynasore: the Dyngo compounds potently inhibit dynamin and endocytosis. *Traffic* **14**, 1272–1289
24. Lefkimmiatis, K., Leronni, D., and Hofer, A. M. (2013) The inner and outer compartments of mitochondria are sites of distinct cAMP/PKA signaling dynamics. *J. Cell Biol.* **202**, 453–462
25. Thul, P. J., Åkesson, L., Wiking, M., Mahdessian, D., Geladaki, A., Ait Blal, H., *et al.* (2017) A subcellular map of the human proteome. *Science* **356**. https://doi.org/10.1126/science.aal3321
26. Uhlén, M., Fagerberg, L., Hallström, B. M., Lindskog, C., Oksvold, P., Mardinoglu, A., *et al.* (2015) Proteomics. Tissue-based map of the human proteome. *Science* **347**, 1260419
27. Tsai, G., and Coyle, J. T. (2002) Glutamatergic mechanisms in schizophrenia. *Annu. Rev. Pharmacol. Toxicol.* **42**, 165–179
28. Schobel, S. A., Chaudhury, N. H., Khan, U. A., Paniagua, B., Styner, M. A., Asllani, I., *et al.* (2013) Imaging patients with psychosis and a mouse model establishes a spreading pattern of hippocampal dysfunction and implicates glutamate as a driver. *Neuron* **78**, 81–93
29. Merritt, K., Egerton, A., Kempton, M. J., Taylor, M. J., and McGuire, P. K. (2016) Nature of glutamate alterations in schizophrenia: a meta-analysis of proton magnetic resonance spectroscopy studies. *JAMA Psych.* **73**, 665–674
30. Li, C.-T., Yang, K.-C., and Lin, W.-C. (2019) Glutamatergic dysfunction and glutamatergic compounds for major psychiatric disorders: evidence from clinical neuroimaging studies. *Front. Psych.* **9**. https://doi.org/10.3389/fpsyt.2018.00767
31. Chen, Y., Wang, Y., Ertürk, A., Kallop, D., Jiang, Z., Weimer, R. M., *et al.* (2014) Activity-induced Nr4a1 regulates spine density and distribution pattern of excitatory synapses in pyramidal neurons. *Neuron* **83**, 431–443
32. Tian, R., Gachechiladze, M. A., Ludwig, C. H., Laurie, M. T., Hong, J. Y., Nathaniel, D., *et al.* (2019) CRISPR interference-based platform for multimodal genetic screens in human iPSC-derived neurons. *Neuron* **104**, 239–255.e212
33. Tewson, P. H., Martinka, S., Shaner, N. C., Hughes, T. E., and Quinn, A. M. (2016) New DAG and cAMP sensors optimized for live-cell assays in automated laboratories. *J. Biomol. Screen* **21**, 298–305
34. Lyons, M. R., and West, A. E. (2011) Mechanisms of specificity in neuronal activity-regulated gene transcription. *Prog. Neurobiol.* **94**, 259–295
35. Benito, E., Valor, L. M., Jimenez-Minchan, M., Huber, W., and Barco, A. (2011) cAMP response element-binding protein is a primary hub of activity-driven neuronal gene expression. *J. Neurosci.* **31**, 18237–18250
36. Chung, L. (2015) A brief introduction to the transduction of neural activity into fos signal. *Dev. Reprod.* **19**, 61–67
37. Lakhina, V., Arey, R. N., Kaletsky, R., Kauffman, A., Stein, G., Keyes, W., *et al.* (2015) Genome-wide functional analysis of CREB/Long-Term memory-dependent transcription reveals distinct basal and memory gene expression programs. *Neuron* **85**, 330–345
38. Zhang, X., Odom, D. T., Koo, S. H., Conkright, M. D., Canettieri, G., Best, J., *et al.* (2005) Genome-wide analysis of cAMP-response element binding protein occupancy, phosphorylation, and target gene activation in human tissues. *Proc. Natl. Acad. Sci. U. S. A.* **102**, 4459–4464
39. Eden, E., Navon, R., Steinfeld, I., Lipson, D., and Yakhini, Z. (2009) GOrilla: a tool for discovery and visualization of enriched GO terms in ranked gene lists. *BMC Bioinform.* **10**, 48
40. Hagena, H., Hansen, N., and Manahan-Vaughan, D. (2016) β-Adrenergic control of hippocampal function: subserving the choreography of synaptic information storage and memory. *Cereb. Cortex* **26**, 1349–1364
41. Taylor, S. S., Wallbott, M., Machal, E. M. F., Søberg, K., Ahmed, F., Bruystens, J., *et al.* (2021) Pka Cβ: a forgotten catalytic subunit of cAMP-dependent protein kinase opens new windows for PKA signaling and disease pathologies. *Biochem. J.* **478**, 2101–2119
42. Uhler, M. D., Chrivia, J. C., and McKnight, G. S. (1986) Evidence for a second isoform of the catalytic subunit of cAMP-dependent protein kinase. *J. Biol. Chem.* **261**, 15360–15363
43. Walker-Gray, R., Stengel, F., and Gold, M. G. (2017) Mechanisms for restraining cAMP-dependent protein kinase revealed by subunit quantitation and cross-linking approaches. *Proc. Natl. Acad. Sci. U. S. A.* **114**, 10414–10419
44. Tsvetanova, N. G., Trester-Zedlitz, M., Newton, B. W., Riordan, D. P., Sundaram, A. B., Johnson, J. R., *et al.* (2017) Protein-coupled receptor endocytosis confers uniformity in responses to chemically distinct ligands. *Mol. Pharmacol.* **91**, 145–156
45. [preprint] Willette, B. K. A., and Tsvetanova, N. G. (2022) Endosome positioning coordinates spatially selective GPCR signaling. *bioRxiv*. https://doi.org/10.1101/2022.07.26.501572
46. Jong, Y.-J. I., Harmon, S. K., and O'Malley, K. L. (2018) Intracellular GPCRs play key roles in synaptic plasticity. *ACS Chem. Neurosci.* **9**, 2162–2172
47. Leung, C. C. Y., and Wong, Y. H. (2017) Role of G Protein-Coupled receptors in the regulation of structural plasticity and cognitive function. *Molecules* **22**, 1239
48. Regard, J. B., Sato, I. T., and Coughlin, S. R. (2008) Anatomical profiling of G protein-coupled receptor expression. *Cell* **135**, 561–571
49. Moreno, J. L., Holloway, T., and González-Maeso. (2013) J. G protein-coupled receptor heterocomplexes in neuropsychiatric disorders. *Prog. Mol. Biol. Transl. Sci.* **117**, 187–205
50. Catapano, L. A., and Manji, H. K. (2007) G protein-coupled receptors in major psychiatric disorders. *Biochim. Biophys. Acta* **1768**, 976–993
51. Monfared, R. V., Alhassen, W., Truong, T. M., Gonzales, M. A. M., Vachirakorntong, V., Chen, S., *et al.* (2021) Transcriptome profiling of dysregulated GPCRs reveals overlapping patterns across psychiatric disorders and age-disease interactions. *Cells* **10**. https://doi.org/10.3390/cells10112967
52. Kandel, E. R. (2012) The molecular biology of memory: cAMP, PKA, CRE, CREB-1, CREB-2, and CPEB. *Mol. Brain* **5**, 14
53. Benarroch, E. E. (2008) Adenosine and its receptors: multiple modulatory functions and potential therapeutic targets for neurologic disease. *Neurology* **70**, 231–236
54. Nikolaienko, O., Patil, S., Eriksen, M. S., and Bramham, C. R. (2018) Arc protein: a flexible hub for synaptic plasticity and cognition. *Semin. Cell Dev. Biol.* **77**, 33–42
55. Miranda, M., Morici, J. F., Zanoni, M. B., and Bekinschtein, P. (2019) Brain-derived neurotrophic factor: a key molecule for memory in the healthy and the pathological brain. *Front. Cell Neurosci.* **13**, 363
56. Loughney, K., Martins, T. J., Harris, E. A., Sadhu, K., Hicks, J. B., Sonnenburg, W. K., *et al.* (1996) Isolation and characterization of cDNAs corresponding to two human calcium, calmodulin-regulated, 3',5'-cyclic nucleotide phosphodiesterases. *J. Biol. Chem.* **271**, 796–806
57. Chang, A., Li, P. P., and Warsh, J. J. (2003) cAMP-Dependent protein kinase (PKA) subunit mRNA levels in postmortem brain from patients

with bipolar affective disorder (BD). *Brain Res. Mol. Brain Res.* **116**, 27–37
58. Chang, A., Li, P. P., and Warsh, J. J. (2003) Altered cAMP-dependent protein kinase subunit immunolabeling in post-mortem brain from patients with bipolar affective disorder. *J. Neurochem.* **84**, 781–791
59. Perez, J., Tardito, D., Mori, S., Racagni, G., Smeraldi, E., and Zanardi, R. (1999) Abnormalities of cyclic adenosine monophosphate signaling in platelets from untreated patients with bipolar disorder. *Arch. Gen. Psych.* **56**, 248–253
60. Tardito, D., Tura, G. B., Bocchio, L., Bignotti, S., Pioli, R., Racagni, G., and Perez, J. (2000) Abnormal levels of cAMP-dependent protein kinase regulatory subunits in platelets from schizophrenic patients. *Neuropsychopharmacology* **23**, 216–219
61. Brennand, K. J., Simone, A., Jou, J., Gelboin-Burkhart, C., Tran, N., Sangar, S., *et al.* (2011) Modelling schizophrenia using human induced pluripotent stem cells. *Nature* **473**, 221–225
62. Wang, S., Rhijn, J. R. V., Akkouh, I., Kogo, N., Maas, N., Bleeck, A., *et al.* (2022) Loss-of-function variants in the schizophrenia risk gene SETD1A alter neuronal network activity in human neurons through the cAMP/PKA pathway. *Cell Rep.* **39**, 110790
63. Sanjana, N. E., Shalem, O., and Zhang, F. (2014) Improved vectors and genome-wide libraries for CRISPR screening. *Nat. Methods* **11**, 783–784
64. Shalem, O., Sanjana, N. E., Hartenian, E., Shi, X., Scott, D. A., Mikkelson, T., *et al.* (2014) Genome-scale CRISPR-Cas9 knockout screening in human cells. *Science* **343**, 84–87
65. Gilbert, L. A., Larson, M. H., Morsut, L., Liu, Z., Brar, G. A., Torres, S. E., *et al.* (2013) CRISPR-mediated modular RNA-Guided regulation of transcription in eukaryotes. *Cell* **154**, 442–451
66. Gilbert, L. A., Horlbeck, M. A., Adamson, B., Villalta, J. E., Chen, Y., Whitehead, E. H., *et al.* (2014) Genome-Scale CRISPR-mediated control of gene repression and activation. *Cell* **159**, 647–661
67. Dobin, A., Davis, C. A., Schlesinger, F., Drenkow, J., Zaleski, C., Jha, S., *et al.* (2013) STAR: ultrafast universal RNA-seq aligner. *Bioinformatics* **29**, 15–21
68. Liao, Y., Smyth, G. K., and Shi, W. (2014) featureCounts: an efficient general purpose program for assigning sequence reads to genomic features. *Bioinformatics* **30**, 923–930
69. Love, M. I., Huber, W., and Anders, S. (2014) Moderated estimation of fold change and dispersion for RNA-seq data with DESeq2. *Genome Biol.* **15**, 550